https://doi.org/10.5194/egusphere-2022-631
Preprint. Discussion started: 25 July 2022

New constraints on the tectonic evolution by subduction of the Bangong Co-Nujiang Tethys Oceanic Basin: Insights from magnetic fabric and U-Pb dating of detrital zircon during the Late Jurassic to Early Cretaceous

Qinglong Chen[a]; Xin Cheng[a]; Feifei Huo[a,b]; Yanan Zhou[a]; Nan Jiang[a,c]; Bitian Wei[a]; Baofeng Wang[a,d]; Pengxiang Xu[a,d]; Dongmeng Zhang[a]; Longyun Xing[a]; Teng Li[a]; Feifan Liu[a]; Jingyue Wu[a]; Jiawei Wang[a]; Hanning Wu[a*]

[a] State Key Laboratory of Continental Dynamics, Department of Geology, Northwest University, Xi'an, 710069, China

[b] College of Engineering, Zunyi Normal University, Zunyi Guizhou 563006, China

[c] College of Petrol and Environment Engineering, Yan'an University, Yan'an 716000, Shaanxi, China

[d] Gansu Provincial Coal Geological Exploration Institute, Lanzhou 730000, China

Correspondence: Qinglong Chen; chenqinglong@stumail.nwu.edu.cn
Hanning Wu; wuhn2506@nwu.edu.cn

Abstract

The subduction process between the Bangong Co-Nujiang Tethys Oceanic Basin and the South Qiangtang Block is one of the key issues in the study of the Tethys domain. In order to clarify the evolution process and achieve tectonic constraints, the clastic rock and limestone in the northern margin of the Lhasa block and the southern Qiangtang block were studied in detail through the study of magnetic fabric and zircon U-Pb dating. The results show that the depositional age of the Shamuluo Formation is 131-95 Ma, belonging to the Late Jurassic-Early Cretaceous; the Sowa Formation is earlier (163.5-157.3 Ma), belonging to the Late Jurassic. The detrital provenances of the Shamuluo and Suowa Formations are mainly from the magmatic arc of the Lhasa block and the cyclic orogenic belt of the South Qiangtang block. The fabrics of sandstones in the Shamuluo Formation and some sandstones in the Suowa Formation

https://doi.org/10.5194/egusphere-2022-631
Preprint. Discussion started: 25 July 2022

belong to sedimentary magnetic fabrics related to paleocurrent; the limestone and other sandstones of the Sowa Formation are subject to stress and deformation, and belong to the strain fabric related to the structure. A comprehensive study of detrital zircon U-Pb geochronology, magnetic fabric and petrography shows that the Bangong Co-Nujiang ocean basin is affected by plate fragmentation, and there is a north-south two-way subduction. The southward subduction changes in polarity at 163.5-157.3 Ma and begins the northward subduction. At 145 Ma, the Bangong Co-Nujiang Tethys Ocean closed, but the central remnant of Bangong Co-Nujiang Oceanic Basin continued to subduct until 131-102.9 Ma.

Keywords

Bangong Co-Nujiang Tethys Oceanic Basin; magnetic fabric; zircon U-Pb dating; Late Jurassic to Early Cretaceous; subduction

1. Introduction

Sedimentary rocks are accompanied by sedimentation, diagenesis and tectonic deformation, and the mineral fabric inside the rocks has experienced the evolution from primary to secondary. The two strain states existing in the tectonic deformation process are related to the folding action of the rock formation. The two strain states have different magnetic fabric characteristics. Ramsay and Huber (1983) proposed the strain deformation model of rock magnetic fabric in the first place, which consists of sedimentary fabric, initial deformation fabric, pencil-like fabric to weakly cleavage magnetic fabric, strong cleavage fabric and tensile linear fabric. Anisotropy of magnetic susceptibility (AMS) is a magnetic fabric testing and analysis technique, which introduced based on the difficulty of fabric analysis related to sedimentary diagenesis and strain deformation. It has been widely used in the tectonic deformation and paleo-stress restoration of orogenic belts (Borradaile and Henry 1997), and the determination of sediment paleocurrent flow and volcanic lava flow (Gurioli et al. 2005; Cifelli et al. 2015). In addition, the combination of detrital zircon U-Pb isotopic geochronology and magnetic fabric technology can constrain the tectonic evolution process to a greater extent. Detrital zircon in sediments records significant tectonic-magmatic events prior to and at the same time as stratigraphic deposition, and can be used to trace sedimentary provenance and tectonic setting discussions (Cawood et al. 2012). It includes reconstruction of paleogeographic environment, restoration of large-scale paleocurrent system; defining the absolute age of the strata, providing the maximum depositional age of the stratum; stratigraphic comparison and reproducing the tectonic environment and evolution of the provenance area, etc.

The subduction process of the Bangongco-Nujiang Tethys Oceanic Basin is an important tectonic activity in the formation and evolution of the Qinghai-Tibet Plateau

https://doi.org/10.5194/egusphere-2022-631
Preprint. Discussion started: 25 July 2022

(Yin and Harrison 2000; Metcalfe 2006, 2013; Xu et al. 2016). With the tectonic evolution and mineral resources research of Neo-Tethys, it has become an important study in the geology field currently. Through different research methods (island arc magma, ophiolitic melange, and disappearance of marine strata, etc.), it is generally believed that the time when the Bangongco-Nujiang Oceanic Basin began to subduct was in the Early and Middle Jurassic-Early Cretaceous (Yin and Harrison, 2000; Guynn et al. 2006; Kapp et al. 2007; Zhang et al. 2014; Zhu et al. 2016), but there are big differences on the specific time division. Bioclastic rocks mixed with OIB-type basalts (120-108 Ma) in the Bangong Co-Nujiang suture zone, supporting the beginning of subduction in the Middle Jurassic (Liu et al. 2014); deep Earth physics and mantle dynamics show that the Bangong Co-Nujiang Oceanic Basin has subducted under the Qiangtang Block at 110 Ma (Kapp et al. 2007); the zircon geochronology of collisional granites shows that the subduction of the oceanic basin is still going on at 120-110 Ma (Li et al. 2022). There are three views on the subduction polarity of the Bangong Co-Nujiang Oceanic Basin, namely northward, southward and north-south direction: (1) MORB-type (-180 Ma), SSZ-type (190-180 Ma) forearc ophiolite in the Early Jurassic (Gyunn et al. 2006; Wang et al. 2016) and high-magnesium andesite represent the arc-trough system under the background of northward subduction of oceanic basins (Whattam and Stern 2011; Ishizuka et al. 2014). (2) The widely developed Mugagangri melange has a forearc basin corresponding to southward subduction. (3) The separation of basalts with high and low calc-alkali content from the volcanic rocks of the North Lhasa Terrane suggests slab gyration and slab fragmentation (Gvirtzman and Nur 1999; Grove et al. 2009). Relying on the circulation of mantle flow, the Bangong Co-Nujiang Oceanic Basin experienced two-way subduction (116-100 Ma) from south to north.

In order to precisely define the subduction time and subduction polarity of the Bangong Co-Nujiang Oceanic Basin, this paper intends to combine the magnetic fabric analysis with the detrital zircon U-Pb isotopic dating. Detailed research on rock magnetism, magnetic fabric and detrital zircon provenance were carried out on the sandstone of the Shamuluo Formation exposed in the Nyima area of the North Lhasa Block and the sandstone and limestone of the Suowa Formation in the Shuanghu area of the South Qiangtang Block. Combined with petrography, paleomagnetic research and paleogeographic environment, the origin of its magnetic formation, formation time of strata, sediment source, subduction time and polarity of oceanic basin are discussed, providing new evidence for the tectonic evolution of the subduction on the Bangong Co-Nujiang Oceanic Basin.

2. Geological background and petrologic features

2.1 Geological background

The sandstone of the Shamuluo Formation exposed in the Nyima area belongs to the northern Lhasa Block, which is an active continental margin deposit with the properties

https://doi.org/10.5194/egusphere-2022-631
Preprint. Discussion started: 25 July 2022

of a residual sea basin under the background of the subduction on the Bangong Co-Nujiang Oceanic Basin (Wu et al. 2021). The sandstone and limestone of the Suowa Formation belong to the South Qiangtang Block, where shelf-shallow water deposits are developed, mainly in the mixed platform environment of carbonate rocks and clastic rocks (Xue et al. 2020). The South Qiangtang Block and the Lhasa Block, as important components of the Qinghai-Tibet Plateau, are divided into north and south sides by the Bangong Co-Nujiang suture zone (Yin and Harrison 2000; Chen et al. 2021). The North Lhasa Block is generally considered to be an island arc block formed during the subduction of the Tethys Ocean, which is a part between the Bangong Co-Nujiang suture zone and the ophiolite belt in Shiquan River-Laguo Co-Yongzhu-Nam Co-Jiali. Volcanic sedimentary strata in the Early Cretaceous are widely developed and covered by red molasse formations in the late Cretaceous. Under the action of ocean-continent collision, the South Qiangtang Block developed a foreland basin during the Jurassic-Early Cretaceous period, which was in unconformity contact with the underlying strata, and was a sand-mudstone flysch deposit, showing an early wedge-shaped sedimentary body in a foreland basin. It gradually transformed into marine molasse deposits from the Middle Jurassic to the Late Cretaceous, which marked the change of the sedimentary properties of the South Qiangtang Block. The Bangong Co-Nujiang suture zone, as the dividing line between the two, represents the remains of the Bangong Co-Nujiang Tethys Ocean (Pan et al. 2012). The evolution process of the Bangong Co-Nujiang suture zone is complex, and the strata are continuously distributed with Jurassic ophiolite, subduction accretionary complex, and intermediate-acid magmatic rocks (Figure 1). The widely developed magmatic rocks in the suture zone and both sides record the geological information of the subduction and closure of the Bangong Co-Nujiang Ocean, the separation of slabs and the delamination of the crust (Zhu et al. 2011, 2016; Hu et al. 2017).

https://doi.org/10.5194/egusphere-2022-631
Preprint. Discussion started: 25 July 2022

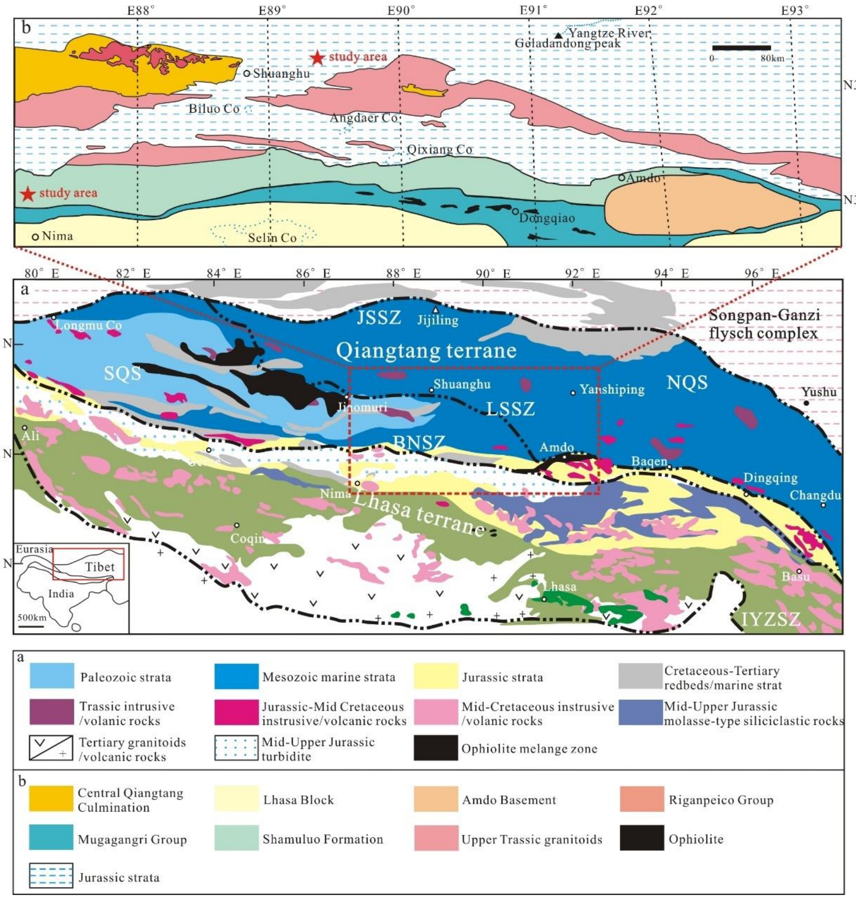

Figure 1. Sedimentary strata, lithological distribution and division of tectonic units shown by the geological background map. (a) Qinghai-Tibet Plateau Geological Map; (b) Geological map of the study area.

2.2 Petrographic features of the Shamuluo Formation

The Shamuluo Formation was originally pointed to the neritic clastic rock formation with rich fossils exposed in the Aweng Co-Salt Lake area. The Shamuluo Formation is exposed to different degrees in the Bangong Co-Nujiang suture zone, which is a combination of clastic rock and limestone. It has an angular unconformity contact with bathyal-abyssal sediments of the underlying Mugagangri Group (Wang et al. 2016). Microscopic observation (Figure 2) shows that the main mineral components of the sandstone of the Shamuluo Formation are: quartz (50%-60%), feldspar (5%), mineral debris (15%-20%) and hetero-bases (15%) -20%). Most of the quartz components come from clastic components and igneous rock components. The clastic quartz contains gas-liquid inclusions (Figure 2(d)), and the enlarged quartz edge of the parent rock is denuded during the transportation process and is irregular residual. The volcanic rocks are irregular in shape, with dissolution harbors and intragranular micro-fractures

https://doi.org/10.5194/egusphere-2022-631
Preprint. Discussion started: 25 July 2022

(Figure 2(f) (g)). Mineral debris contains muscovite, and the interference color is bright under cross-polarized light; tuff debris contains feldspar and quartz crystal debris of varying sizes; chlorite appears pale green and pale yellow under a single polarizer. The hetero-bases are mainly carbonate stucco, and the crystal grains with brighter interference color appear locally. In addition to quartz, pyroclastic rocks include extrusive rock gravel (porphyritic structure, quartz phenocryst dissolution), extrusive rock debris (plagioclase microcrystalline oriented arrangement, mixed with magnetite), tuff debris (contain feldspar and quartz crystals of different sizes) and a small amount of muscovite and chlorite (Figure 2(f) (g)).

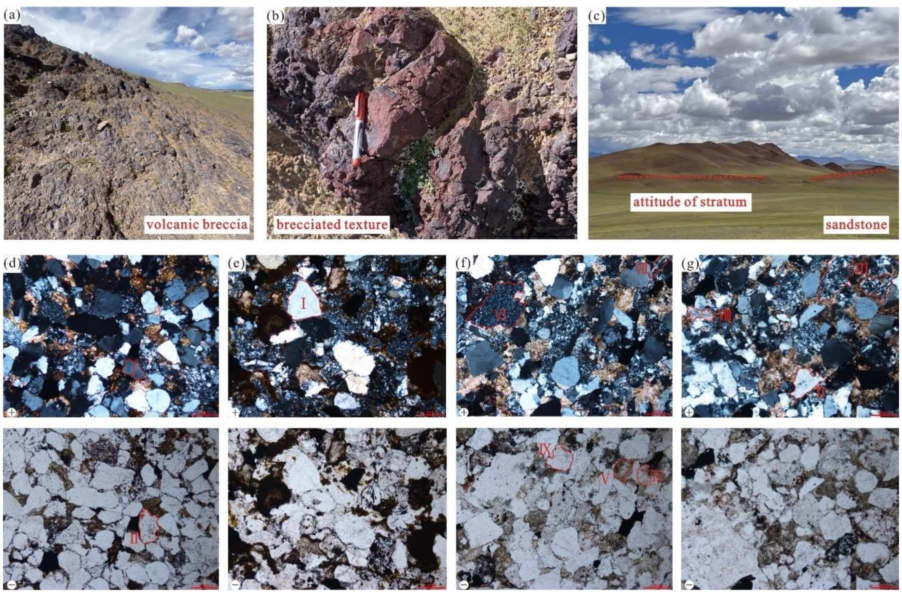

Figure 2. Field and petrographic photos of the Shamuluo Formation. (a) (b) pyroclastic rocks of the Shamuluo Formation; (c) sandstone of the Shamuluo Formation; Mineral code: I, detrial quartz; II, fluid inclusion; III, magnetite; IV, clay mineral; V, chlorite; VI, tuff debris; VII, anorthose; VIII, white mica; IX, volcanic quartz.

2.3 Petrographic features of the Suowa Formation

The lithology of the lower member of the Suowa Formation is red-gray micrite and bioclastic micrite, and the upper member of the Suowa Formation is argillaceous siltstone. Micrite limestone and bioclastic limestone are interbedded with unequal thickness, mixed with thin shell limestone. The sandstone develops parallel bedding and ripple marks, and the silty mudstone contains sporopollen and dinoflagellate fossils. Microscopic observation shows (Figure 3) that the main mineral components of the Sowa Formation sandstone are: quartz (60%-70%), feldspar (5%), mineral debris (10%) and hetero-bases (15%-25%). Quartz is mainly "recycling" quartz and volcanic rock (Figure 3(d)), "recycling" quartz has no cleavage, and has gas-liquid inclusions and regrowth phenomena; volcanic rocks are irregular in shape and have dissolved edges. The feldspar type is potassium feldspar with obvious cleavage development. The

https://doi.org/10.5194/egusphere-2022-631
Preprint. Discussion started: 25 July 2022

mineral debris is mainly composed of muscovite with bright interference color, the hetero-bases is mainly extrusive rock debris, and a small amount of mudstone debris. The extrusive rock fragments have obvious crystalline oriented arrangement and contain dark minerals such as magnetite; the mudstone debris is dominated by clay minerals, and there is no directional structure. There are obvious cracks on the mineral crystal surface of sample J3A0507-2 (Figure 3(e)), which are related to the stress deformation.

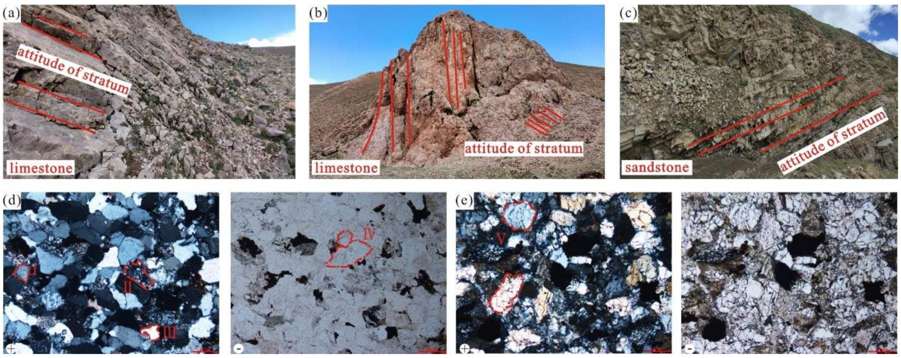

Figure 3. Field and petrographic photos of the Suowa Formation. (a) (b) limestone of Suowa Formation; (c) sandstone of Suowa Formation; Mineral code: I, potassium feldspar; II, magnetite; III, volcanic quartz; IV, fluid inclusion; V, stress deformation.

3. Sample collection and testing

3.1 Sample collection

Sample collection was carried out at relevant sections in the Nyima area of the Lhasa block and Shuanghu area of the South Qiangtang Basin. The samples of the Shamuluo Formation were collected on a continuous profile in the North Lhasa Block, and the profile position is 32°02′02″N, 87°04′07″E. The lithology is mainly silty mudstone, argillaceous siltstone (sampling site number JS01-04) and pyroclastic rock (sampling site number JS05); the samples of the Suowa Formation were collected in two profiles in the South Qiangtang Basin, and the profiles are located at 33°08′07″N, 89°00′43″E, respectively. The lithology is silty mudstone, argillaceous siltstone (sampling site named J3A) and micrite limestone (sampling site named J3B). 34 pieces of sandstone and 36 pieces of pyroclastic rocks were collected from the Shamuluo Formation. 21 pieces of limestone and 69 pieces of sandstone from the Suowa Formation were collected. All samples were drilled in the field with a portable gasoline drilling rig, oriented and sampled with an orientator and a magnetic compass. Standard cylindrical samples with a height of 2.2 cm were then cut indoors, and the remainder was used for rock magnetic analysis and detrital zircon U-Pb dating studies.

3.2 Analytical methods

https://doi.org/10.5194/egusphere-2022-631
Preprint. Discussion started: 25 July 2022

The test analysis of the magnetic fabric samples was accomplished at the State Key Laboratory of Continental Dynamics, Northwest University. Magnetic fabric analysis was carried out at room temperature and low field (temperature 298K, working in low field) with Kappabridge magnetic susceptibility meter from Czech AGICO (MFK1-FB, test field strength 300A m-1, detection limit 2×10^{-8}SI, test accuracy 1%, Frequency 975Hz) to complete the test of magnetic susceptibility anisotropy. The test results are processed by Anisoft 4.2 software, and the test results are shown in Table 1. Rock magnetic experiments include magnetic susceptibility curve with temperature (K-T) and saturation isothermal remanence experiment (SIRM). The change of magnetic susceptibility with temperature experiment was carried out on the multi-frequency magnetic susceptibility instrument of MFK1-FA Kappabridge. The sample was heated from room temperature to 700 °C, and then gradually cooled to room temperature. The main magnetic-carrying minerals in the sample were judged by the relationship curve of magnetic susceptibility and temperature obtained in the whole process. And both the heating and cooling processes are carried out in an argon atmosphere, which reduces the degree of oxidation of the magnetic minerals during the heating process. The isothermal remanence experiment (IRM) judges the types of magnetic minerals in the sample according to the change characteristics of the curve with the increase of the external field through the magnetization curve of forward field and the demagnetization curve of reverse field. After the saturation isothermal remanence (SIRM) is obtained, the obtained isothermal remanence is cleaned by applying a reverse field to the sample. The increase of the field was done with an ASC IM-10-30 pulsed magnetometer, and the measurement was performed with a JR-6A two-speed rotating magnetometer.

The zircon U-Pb isotope dating test has successively completed sample selection, zircon target making, microscopy (reflected light and transmitted light), cathodoluminescence (CL) photography and laser ablation (LA- ICP-MS) in the Nanjing Hongchuang Geological Exploration Technology Service Co. Ltd. Before the test, the crystal morphology and internal structure characteristics of zircon were observed according to the transmitted light, reflected light and CL images. Avoiding cracks and inclusions, the zircon with clear rings and good crystal structure chooses for testing. Data processing includes the selection of sample and blank signals, sensitivity drift correction of instrument, element content and U-Th-Pb isotope ratio and age calculation. In the U-Pb isotope dating, the international standard zircon 91500 and Australian zircon GJ-1 were used as external standards for isotope fractionation correction. For the drift of U-Th-Pb isotope ratio related to the analysis time, the change of 91500 was used for linear interpolation (Liu et al. 2010).

4. Analytical results

4.1 Morphological characteristics of zircon

The color of zircon is mainly gray-white and light yellow, and some are light red in the

https://doi.org/10.5194/egusphere-2022-631
Preprint. Discussion started: 25 July 2022

sandstone and pyroclastic samples of the Shamuluo Formation. The morphology of zircon particles is euhedral or subhedral, and some incomplete particles are irregular, which may be related to the mechanical crushing during the handling process. Sampling points of sandstone and pyroclastic rock have zircon grains with high roundness, which are related to long-distance transportation. The well-preserved zircon particles at the sampling point JS01-04 are ellipsoid and short columnar, and the long axis of the complete zircon particles is 100 µm and the short axis is about 30-50 µm (Figure 4). The zircon particles at the JS05 sampling point are more long cylindrical shape, and the maximum long axis can reach 200µm (Figure 5). Most of the zircon bands are obvious, and the band morphology of the sampling point JS05 is more obvious than that of JS01-04. A few incanus-bright white other-shaped particles with weak bands or no obvious structure were related to Th4+ loss caused by metamorphic recrystallization. There are also a small number of zircons showing a core-edge structure, with an oscillating ring at the core and a gray-white acyclic structure at the edge, reflecting the late growth of zircon by different origins (Xu et al. 2010).

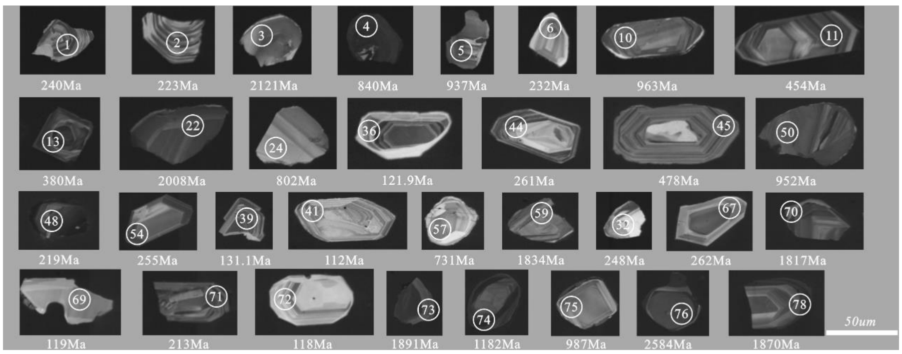

Figure 4. Representative zircon cathodoluminescence images of sedimentary clastic rocks (JS01-04) in the Shamuluo Formation.

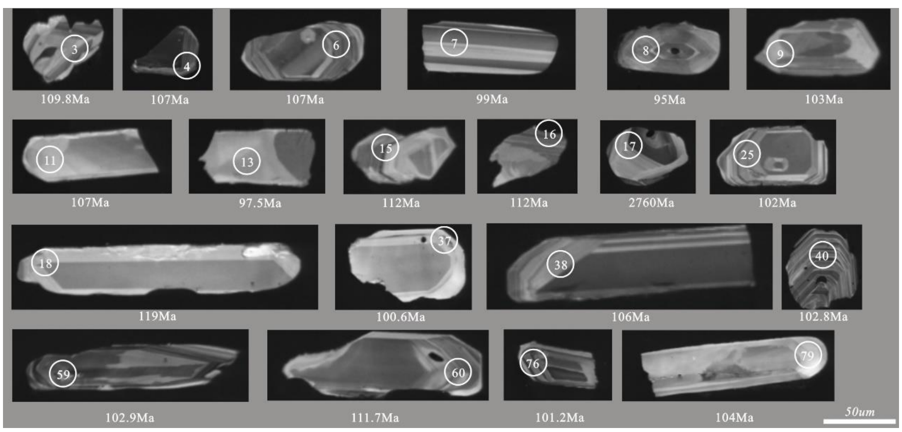

Figure 5. Representative zircon cathodoluminescence images of the pyroclastic rock (JS05) in the Shamuluo Formation.

It is generally believed that the differences in the content of Th and U and the value of

https://doi.org/10.5194/egusphere-2022-631
Preprint. Discussion started: 25 July 2022

Th/U in zircon are related to the genesis of zircon. The content of Th and U in magmatic zircon is generally higher, and the value of Th/U is larger than 0.4; the content of Th and U in metamorphic zircon is low, and the Th/U value is small, less than 0.1 (Hermann J et al. 2001). The distribution range of Th/U value of JS01-04 zircon particles at the sampling point is 0.09-2.11, only one particle is less than 0.1, and most particles are greater than 0.4. At the same time, there are few metamorphic zircon grains in the ringless or weak ring, and most of the particles have obvious oscillation rings, which are typical magmatic zircon. The Th/U value of the sampling point JS05 is generally greater than 0.5, and the oscillation ring is clearer than that of JS01-04. It is believed that the zircon particles of JS05 are more affected by magmatic origin.

4.2 Characteristics of zircon age distribution

For the JS01-04 and JS05 samples, the zircon particles with suitable size, shape and clear oscillation ring were selected for laser ablation. The test data show that the concordance of the two sampling points is extremely high, and the surface ages of 206Pb/238U, 207Pb/235U and 207Pb/206U of all valid test points are basically the same, indicating the data has high reliability. The youngest and oldest zircon obtained from JS01-04 are 112 Ma and 2584 Ma respectively, and the youngest and oldest zircon obtained from JS05 are 95 Ma and 2760 Ma respectively. There are 7 peaks of zircon in JS01-04 sampling point (Figure 6(b)), which are concentrated at 112-131 Ma, 213-380 Ma, 415-480 Ma, 627-840 Ma, 902-987 Ma, 1816-1923 Ma and 2417-2584 Ma respectively. There is only one peak of zircon in the JS05 sampling point, which is concentrated in 95-116Ma, and the weighted average age is 102.9 Ma (Figure 6(c)).

The distribution histogram of zircon U-Pb isotopic age at the two sampling points shows that relatively new age zircon grains account for a larger proportion in the sample (Figure 6(b)(d)). The number of zircon grains at sampling point JS01-04 is the largest in the age range of 100-500 Ma, followed by the number of 600-1000 Ma, and the least in 1800-2000 Ma and 2500 Ma. The zircon particles at the sampling point JS05 are basically all distributed at 90-120 Ma. From the distribution characteristics of overall age and grain morphology of these zircon grains, it can be seen that the sedimentary source area of the sandstone in the Shamuluo Formation isn't single. Mainly from stable provenance areas in the range of 100-500 Ma and 600-1000 Ma, and there are also transports from other provenance areas (1800-2000 Ma and 2500 Ma). Detrital zircon has both highly rounded particles associated with long-distance transportation and euhedral particles with less rounded and sharp edges due to short-distance transportation.

https://doi.org/10.5194/egusphere-2022-631
Preprint. Discussion started: 25 July 2022

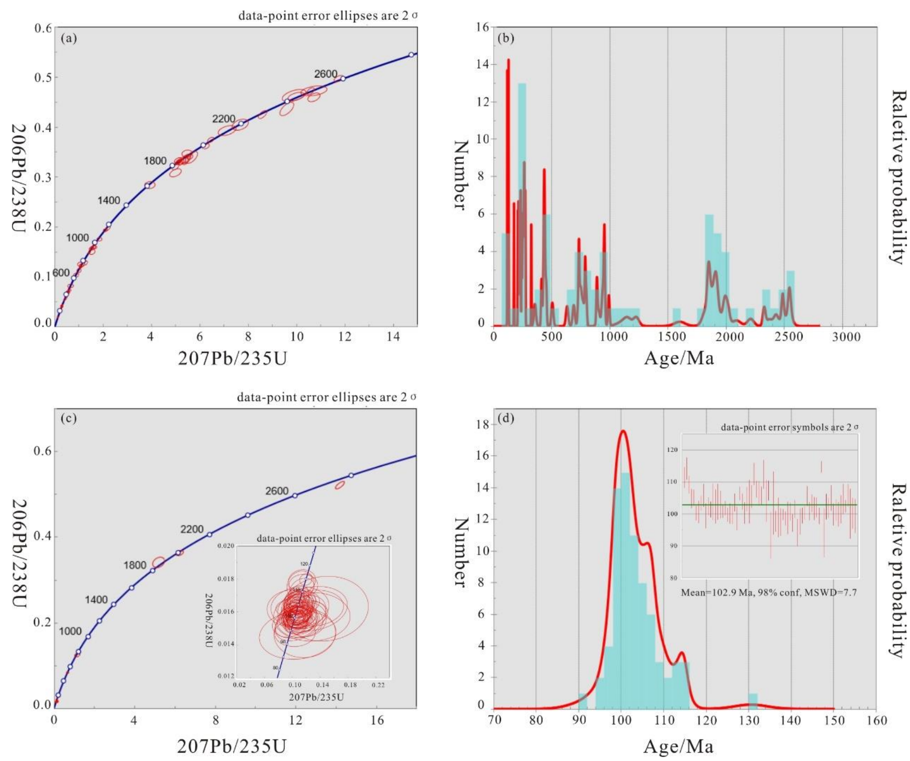

Figure 6. Zircon U-Pb dating harmony map and weighted average age map of sedimentary clastic rocks (JS01-04) (a) (b) and pyroclastic rocks (JS05) (c) (d) in the Shamuluo Formation.

4.3 Rock magnetism

4.3.1 Magnetic susceptibility curve with temperature change (K-T)

Different magnetic minerals show different characteristics during heating and cooling, and the type and size of magnetic minerals can be identified according to their characteristics (Hrouda 1994; Van and Dekkers 1999). The K-T curve can effectively characterize the changes of magnetic minerals and particle size during heating (Ao and Deng 2007). The experimental results of samples from the Shamuluo Formation and the Suowa Formation show that the magnetic susceptibility values of all samples show a downtrend as a whole with the increase of temperature, indicating that there are paramagnetic minerals in the samples. The magnetic susceptibility increases significantly around 400°C, and the magnetic susceptibility peak appears, indicating that there is a phase transition of magnetic minerals, which may be caused by the transformation of some magnetic sulfides into pyrrhotite (Fe_3S_4) (Figure 7). The magnetic susceptibility value of some samples dropped significantly at around 540℃, which is related to the transformation of the high magnetic susceptibility minerals with poor thermal stability into low magnetic susceptibility minerals due to thermal

https://doi.org/10.5194/egusphere-2022-631
Preprint. Discussion started: 25 July 2022

decomposition of pyrrhotite (Fe_3S_4). There are also samples whose magnetic susceptibility values drop around 580 °C, indicating the presence of magnetite in the samples (Figure 7). At the same time, the “Hopkinson” peak generated during the heating of the sample indicates that there may be relatively small magnetic particles (SD) in the sample (Ao and Deng 2007); there are also weak “Hopkinson” peaks under the influence of larger magnetic particles (MD) (J3A0104 and J3A0402). The cooling curves of all samples are higher than the heating curves, indicating that the heating and cooling processes are irreversible. The cooling curves of all samples increased significantly at around 580 °C, indicating that magnetite was produced during the cooling process. Experiments show that the magnetic minerals in the samples are mainly magnetite and paramagnetic minerals, and more magnetite is produced during the heating and cooling process than before the experiment.

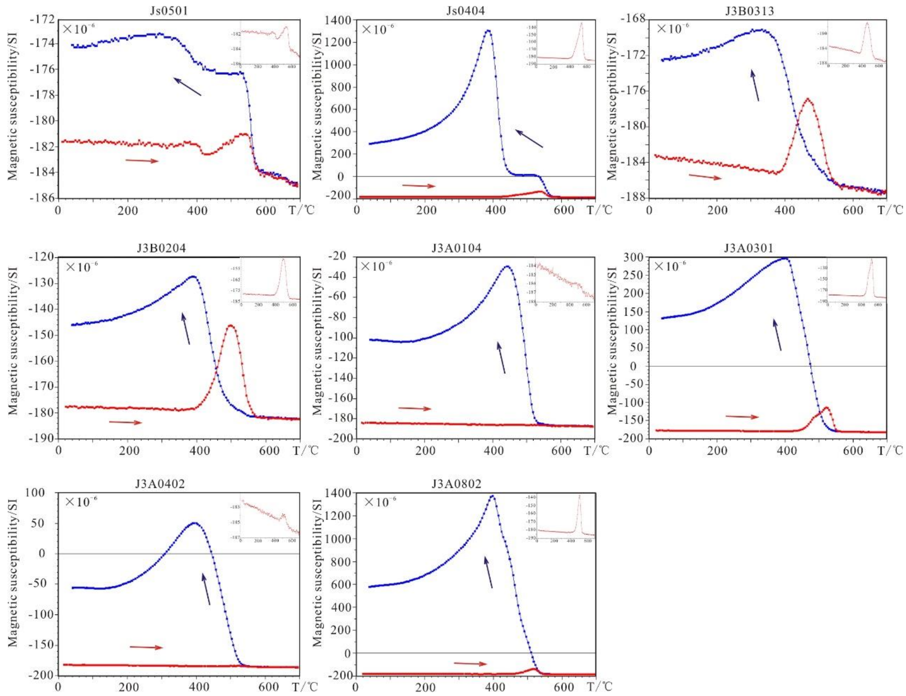

Figure 7. Magnetic susceptibility curves of samples from the Shamuluo and Suowa Formations with temperature change.

4.3.2 Saturation isothermal remanence experiment (SIRM)

The saturation isothermal remanence experiment (SIRM) uses the characteristic that magnetic minerals tend to saturate with the increase of the external field, and preliminarily determines the type of magnetic minerals in the sample through the curve characteristics. The curves of sandstone samples in the Suowa Formation show that the magnetization intensity increases rapidly with the increase of the external field at the initial stage. When the strength of external field is less than 300mT, the magnetization intensity of the sample gradually approaches saturation, indicating that the magnetic

https://doi.org/10.5194/egusphere-2022-631
Preprint. Discussion started: 25 July 2022

minerals in the sample are mainly low-coercivity magnetic minerals. The magnetization intensity of limestone from the Suowa Formation and sandstone from the Shamuluo Formation did not reach saturation at 2T, indicating that the magnetic minerals are relatively simple and mainly high-coercivity magnetic minerals. The demagnetization curve of the reverse field also shows that the magnetic minerals of sandstone samples from the Suowa Formation have low coercivity, and limestone from the Suowa Formation and sandstone from the Shamuluo Formation have high coercivity (Figure 8).

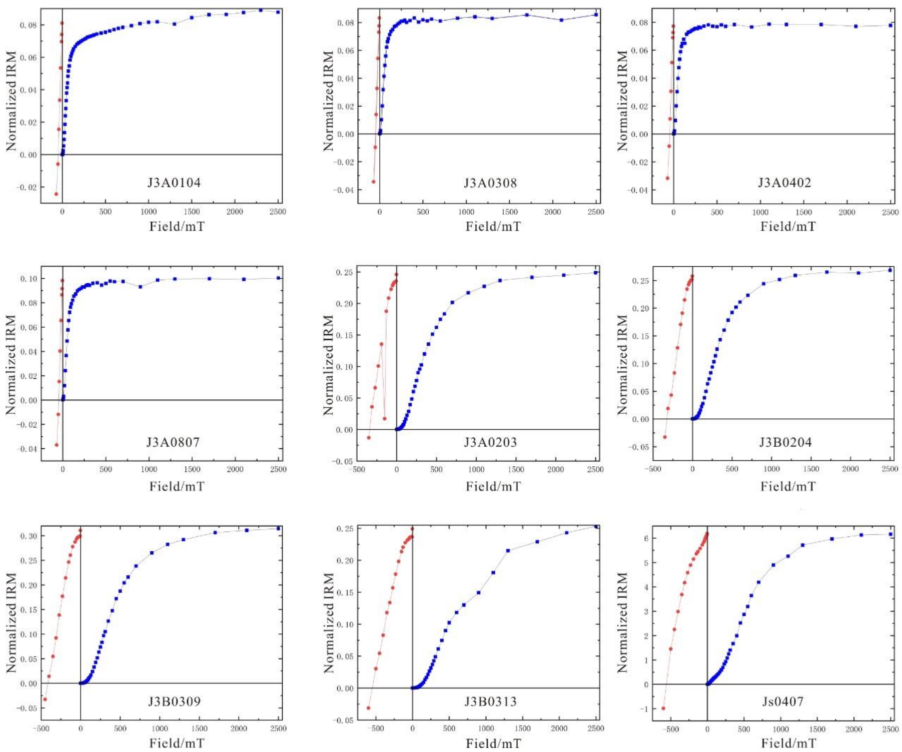

Figure 8. Curves of saturation isothermal remanence.

4.4 Characteristics of magnetic susceptibility and magnetic fabric

The three main axes (K1, K2, K3) of the magnetic susceptibility ellipsoid correspond to the maximum, middle and minimum axes of the sample respectively, and the relevant parameters of magnetic fabric can be obtained from the magnetic susceptibility main axes. The average magnetic susceptibility (Km) reflects the comprehensive characteristics of the magnetic susceptibility of the sample, which is related to the type and distribution of magnetic minerals (Liang et al. 2009); anisotropy (Pj) reflects the orderly degree of sediment particle arrangement, which is controlled by the strength and stability of depositional dynamics (Kong et al. 2018), and reflects deformation

https://doi.org/10.5194/egusphere-2022-631
Preprint. Discussion started: 25 July 2022

information of sample together with shape factor (T); magnetic foliation (F=K2/K3) reflects the degree of surface distribution of sediment particles; magnetic lineation (L=K1/K2) reflects the linear arrangement of the long axis of sediment particles (Gao et al. 2022).

4.4.1 Characteristics of magnetic susceptibility

The Km value of the Shamuluo Formation is 135×10^{-6} SI and the maximum is 145×10^{-6} SI. The Km value of the limestone in the Suowa Formation is -2.26×10^{-6} SI, the two sampling points are negative, and the maximum value is 184×10^{-6} SI. The Km value of the sandstone in the Suowa Formation is 46.3×10^{-6} SI, the maximum value is 82.2×10^{-6} SI, and other sampling points are concentrated at 34.3×10^{-6} SI. The normal sedimentary fabric is mainly affected by hydrodynamics and gravity, and the Pj is relatively small; deformation fabric produced by stress deformation, and the Pj is relatively large. The Pj of sandstones in the Shamuluo Formation is less than 1.06, which is affected by sedimentation; there are samples with Pj less than1 or Pj greater than 1.06 in both the limestone and sandstone of the Suowa Formation, indicating the existence of sedimentary fabric and stress-deformation fabric. The T values of the samples from the Shamuluo Formation are all greater than 0 and less than 1, indicating that the development of magnetic foliation is dominant; however, the average T value of the limestone and sandstone samples in the Suowa Formation is greater than -1 and less than 0, and the T value of individual sampling points is greater than 0, indicating that the development of magnetic lineation is more common and more stressed (Table 1).

Table 1. Magnetic susceptibility parameters of samples in the room temperature (RT) from the northern margin of Lhasa and the South Qiangtang Basin

Sampling point	*N*	*Km*	*L*	*F*	*Pj*	*T*	*K1*	*K2*	*K3*
JS01	10	1.30×10-4	1.001	1.003	1.006	0.316	268.1/6.0	359.1/8.8	144.4/79.3
JS02	13	1.44×10-4	1.002	1.004	1.006	0.276	289.5/0.5	19.5/0.1	123.0/89.5
JS03	5	1.42×10-4	1.001	1.003	1.004	0.274	261.7/15.9	4.9/38.6	153.9/47.1
JS04	6	1.19×10-4	1.002	1.003	1.005	0.218	199.4/4.7	290.1/8.0	79.4/80.7
Shamuluo （average value）	34	1.35×10-4	1.002	1.003	1.005	0.277	265.5/5.2	356.0/6.2	135.7/81.9
J3B01	6	1.84×10-4	1.106	1.046	1.162	-0.312	241.6/35.4	68.8/54.4	334.0/3.4
J3B02	6	-1.82×10-6	0.833	1.005	0.924	-0.042	323.4/13.7	53.0/2.2	152.7/76.1
J3B03	9	-4.18×10-6	0.807	0.918	0.933	0.120	3.6/28.1	118.2/37.8	247.6/39.3
Suowa limestone （average value）	21	-2.26×10-6	0.900	0.979	0.996	-0.050	338.6/12.5	80.3/42.3	235.7/45
J3A01	8	3.54×10-5	1.004	1.006	1.010	0.239	293.9/45.1	201.4/2.5	109.0/44.8
J3A02	6	5.76×10-5	1.052	1.006	1.065	-0.238	98.0/59.3	263.4/29.9	357.1/6.4
J3A03	7	4.62×10-5	1.009	1.004	1.014	-0.228	220.4/77.6	101.8/6.0	10.7/10.8
J3A04	9	3.43×10-5	1.003	1.004	1.007	0.109	204.1/0.1	294.1/37.0	114.0/53.0
J3A05	7	3.43×10-5	1.003	1.006	1.010	0.326	354.4/15.7	254.7/30.8	107.7/54.67
J3A06	7	3.14×10-5	1.004	1.006	1.010	0.166	171.7/2.0	262.5/20.3	76.2/69.611
J3A07	11	2.92×10-5	1.006	1.006	1.013	-0.008	338.6/22.6	246.6/5.0	144.9/66.8

https://doi.org/10.5194/egusphere-2022-631
Preprint. Discussion started: 25 July 2022

J3A08	14	8.22×10-5	1.011	1.003	1.016	-0.520	351.5/78.1	213.3/8.9	122.1/7.8
Suowa sandstone （average value）	69	4.63×10-5	1.010	1.005	1.017	-0.060	351.2/76.2	106.6/6.0	197.9/12.3

The Pj-T diagrams (Figure 9(b)(d)) show that with the increase of magnetic susceptibility anisotropy, the ellipsoid transforms from a flattened to an elongated type, which is associated with strong stress deformation. There are both elongated and flattened ellipsoids in the Figure 9(a), reflecting the initial deformation state of the deposition. It may indicate that there is a weak strain in the deposition state, which makes the ellipsoid transform from a flattened to an elongated shape, but with the stop of the strain, the flattened state is restored, and the whole is still in a relatively stable depositional state (Figure 9(c)). The Flinn diagram (Figure 10) shows that the samples of the Shamuluo Formation are concentrated in the development region of magnetic foliation (K<1), and the magnetic susceptibility ellipsoid is oblate, which is the initial sedimentary fabric. For the sandstone of the Suowa Formation, the samples at three sampling points are located in the area where the magnetic lineation is developed (K>1). The tensile magnetic susceptibility ellipsoid represents the tensile lineation and reflects the strain state. The other five sampling points are located in the magnetic foliation relatively developed area (K < 1), representing the initial deformation fabric. For the limestone of the Suowa Formation, the samples from three sampling points are all located in the area where the magnetic lineation is developed (K>1). The development of magnetic lineation is better than that of magnetic foliation, which is characterized by pencil-like fabric or weak cleavage fabric, reflecting that the initial deposition state and strain effect is increased by stress.

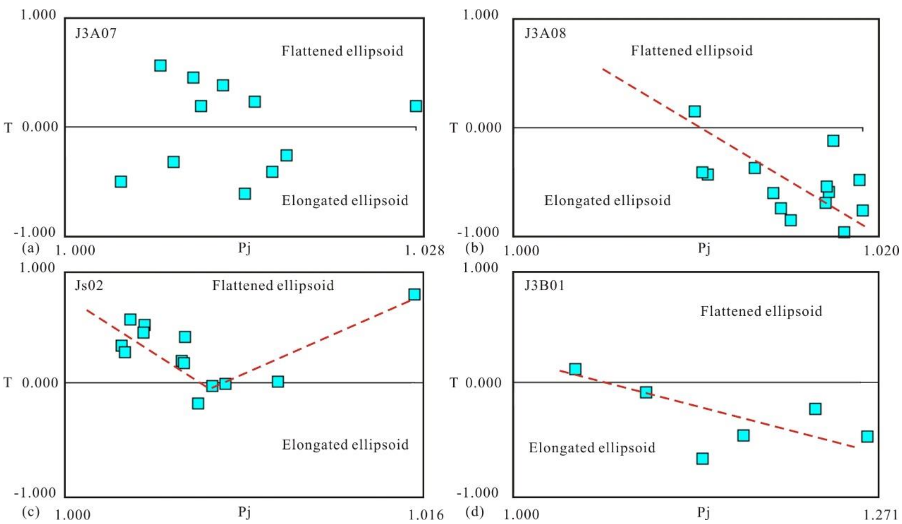

Figure 9. Pj-T diagrams of typical samples. (a) Sandstone of Suowa Formation, sampling point 7; (b) Sandstone of Suowa Formation, sampling point 8; (c) Sandstone of Shamuluo Formation, sampling point 2; (d) Limestone of Suowa Formation, sampling point 1.

https://doi.org/10.5194/egusphere-2022-631
Preprint. Discussion started: 25 July 2022

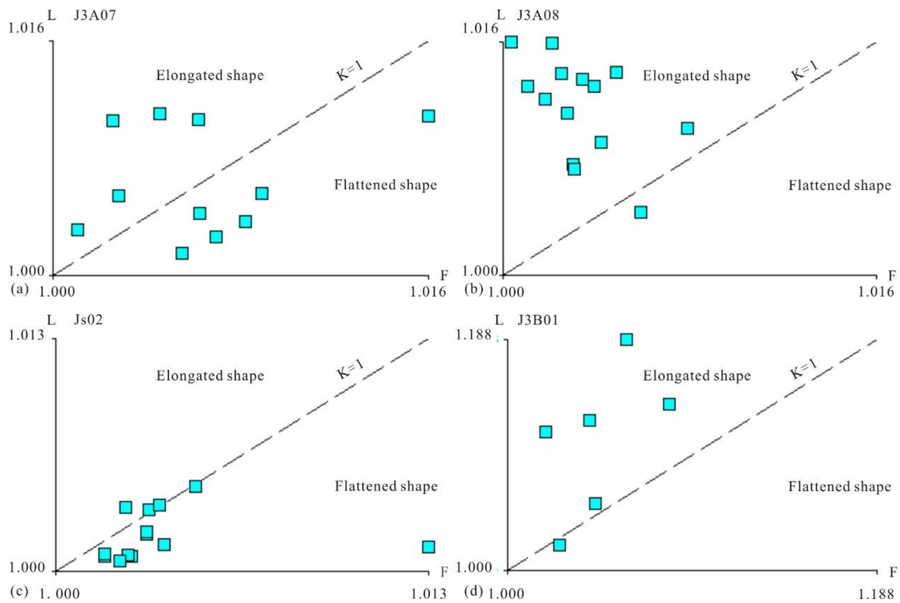

Figure 10. Flinn diagrams of typical samples. (a) Sandstone of Suowa Formation, sampling point 7; (b) Sandstone of Suowa Formation, sampling point 8; (c) Sandstone of Shamuluo Formation, sampling point 2; (d) Limestone of Suowa Formation, sampling point 1.

4.4.2 Characteristics of magnetic fabric

The characteristics of magnetic fabric (stratigraphic correction) in the Shamuluo Formation (Figure 11(a)) show that the minimum axis (K3) of magnetic susceptibility is concentrated near the center of the base circle of the stereographic projection, indicating that the average value of the magnetic foliation is parallel to the stratum, but not completely concentrated near the center of the circle. The maximum axis (K1) of magnetic susceptibility is scattered around the base circle, and comprehensively appears as a flattened magnetic susceptibility ellipsoid, reflecting the characteristics of sedimentary fabric. The characteristics of the limestone magnetic fabric (stratigraphic correction) in the Suowa Formation (Figure 11(b)) show that the maximum axis (K1) of magnetic susceptibility is concentrated in the stratigraphic strike direction, and the minimum axis (K3) is banded and scattered in the direction of layer shortening, which is vertical with the maximum axis (K1), indicating that the magnetic minerals have rotated. The orientation of magnetic lineation is concentrated in NE or NW. The inclination angle of NE direction is smaller at about 0°-3°, and the inclination angle of NW direction is larger. The sandstone magnetic fabric (stratigraphic correction) of the Suowa Formation is characterized by three types, initial deformation fabric or sedimentary fabric (Figure 11(d)) and tensile lineation fabric (Figure 11(c)). In the initial deformation fabric and sedimentary fabric, the minimum axis (K3) of magnetic susceptibility is basically concentrated at the center of the base circle, and the maximum axis (K1) is scattered around, corresponding to the strike direction of the formation.

https://doi.org/10.5194/egusphere-2022-631
Preprint. Discussion started: 25 July 2022

The tensile lineation shows that the maximum axis (K1) of magnetic susceptibility is distributed in the center of the base circle, concentrated in the structural direction, and shows a strong strain state.

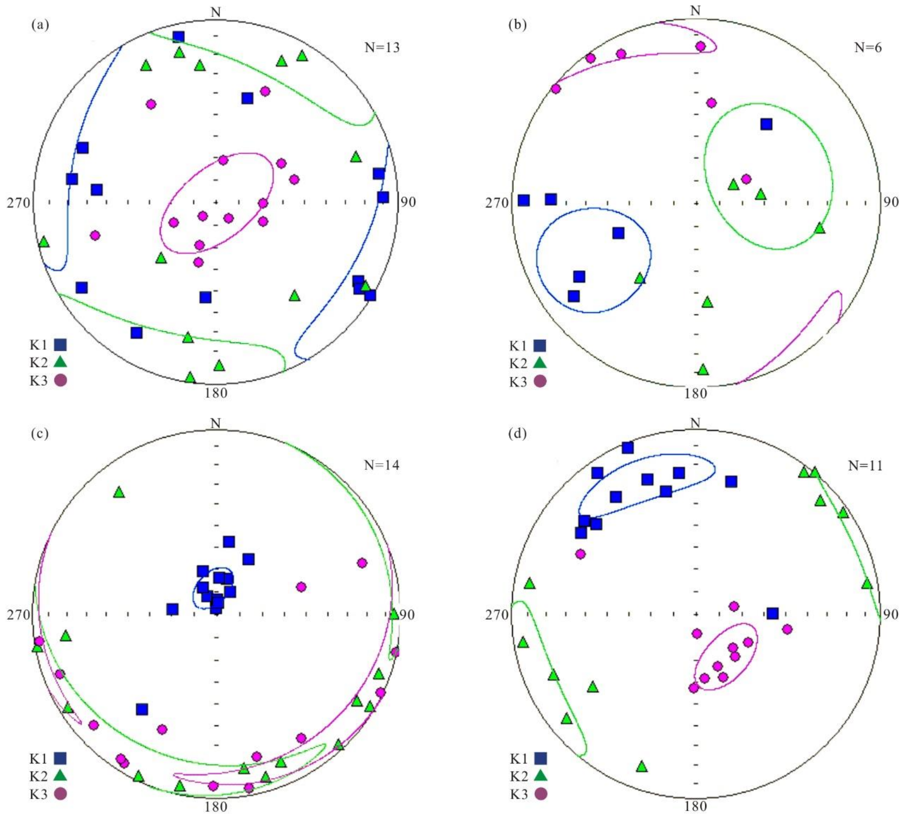

Figure 11. Typical characteristics of magnetic fabric (stratigraphic correction). (a) Sedimentary magnetic fabric at sampling point 2 of sandstone in Shamuluo Formation; (b) pencil-like magnetic fabric at sampling point 1 of limestone in Suowa Formation; (c) tensile magnetic fabric at sampling point 8 of sandstone in Suowa Formation; (d) initial deformation magnetic fabric at sampling point 7 of sandstone in the Suowa Formation.

5. Discussions

5.1 Relationship of stratigraphic ages between the Shamuluo Formation and the Suowa Formation

The Shamuluo Formation and the Suowa Formation in the study area represent the Bangong Co-Nujiang Tethys Oceanic Basin and the South Qiangtang Block,

https://doi.org/10.5194/egusphere-2022-631
Preprint. Discussion started: 25 July 2022

respectively. The tectonic study of these two blocks plays a key role in the constraints of ocean-continent collision. But whether the two developed in the same geological historical period, or whether they developed successively, is the precondition to constrain the tectonic evolution. From west to east of the Bangong Co-Nujiang suture zone, it was collected the *Mesorbitlina sp.* and gastropod *Palarbitolina cf. lenticularis* from the Early Cretaceous (Blumenbach) (Xie et al. 2009), ultra-microfossils *Lotharingius contractus*, *Cyclagelosphaera margerelii*, *Thamnoseris*, *Actinastrea* from Late Jurassic and *Stylosmilia*, *Stylna* from Early Cretaceous. Huang et al. (2017) obtained a weighted average age of detrital zircon at 135.6 ± 2.5 Ma from the Shamuluo Formation in eastern Gerze County, Wu et al. (2021) found the Zargo andesite in the Shamuluo Formation with a zircon crystallization age at 141.3 ± 1.7 Ma. It is believed that the Shamuluo Formation was formed in the period of Late Jurassic-Early Cretaceous. The zircon grains of the Shamuluo Formation at the two sampling sites in this paper are mainly concentrated in 112-131 Ma and 95-116 Ma, respectively, indicating that more zircon grains came from magmatic eruptions in the Early Cretaceous.

Two types of brachiopods and bivalves have been found in the lower part of the Suowa Formation in the South Qiangtang Block. The brachiopods include *Radulopecten fibrosus*, *Gervillella aviculoides*, *Gryphaea bennigi*, and the bivalves include *Lacunosella cf. blanowicensis*, *Pentithyris sp.*, *Biceptirhynchia sp*. These two types of fossils belong to the Oxford period in the Tethys Sea, and the specific age is 163.5-157.3 Ma in the late Oxford period. There are a lot of ammonite fossils from Late Jurassic in the exposed strata of the upper Suowa Formation, including *Virgatosphinctes multifasciatus*, *V. haydeni*, *Blanfordiceras criki* and so on. Among them, *Virgatosphinctes multifasciatus* and *V. haydeni* are the standard molecules of the Tithonian period in Late Jurassic. The Oxfordian or Tithonian periods corresponds to the Late Jurassic (Figure 12), although most scholars believe that the upper part of the Suowa Formation belongs to the Late Jurassic-Early Cretaceous (Fu et al. 2021). However, in this paper, the detrital zircon of the Shamuluo Formation has no crystallization time corresponding to 163.5-157.3 Ma, and more of it is in the time range of 95-130 Ma. This indicates that the Shamuluo Formation may have been deposited at the same time as the Suowa Formation in the South Qiangtang Block in other areas of the suture zone. For example, the granodiorite dikes at 151 ± 2 Ma intruded into the Shamuluo Formation was discovered by Ma et al. (2018) and the clastic rocks at 143 Ma and 163 Ma of the Shamuluo Formation was discovered by Li et al. (2017). However, the clastic stratum of the Shamuluo Formation studied in this paper is slightly later than that of the Suowa Formation, which also confirms the previous view of the "through-time closure" on Bangong Co-Nujiang Tethys Ocean (Fan et al. 2015; Wu et al. 2015).

https://doi.org/10.5194/egusphere-2022-631
Preprint. Discussion started: 25 July 2022

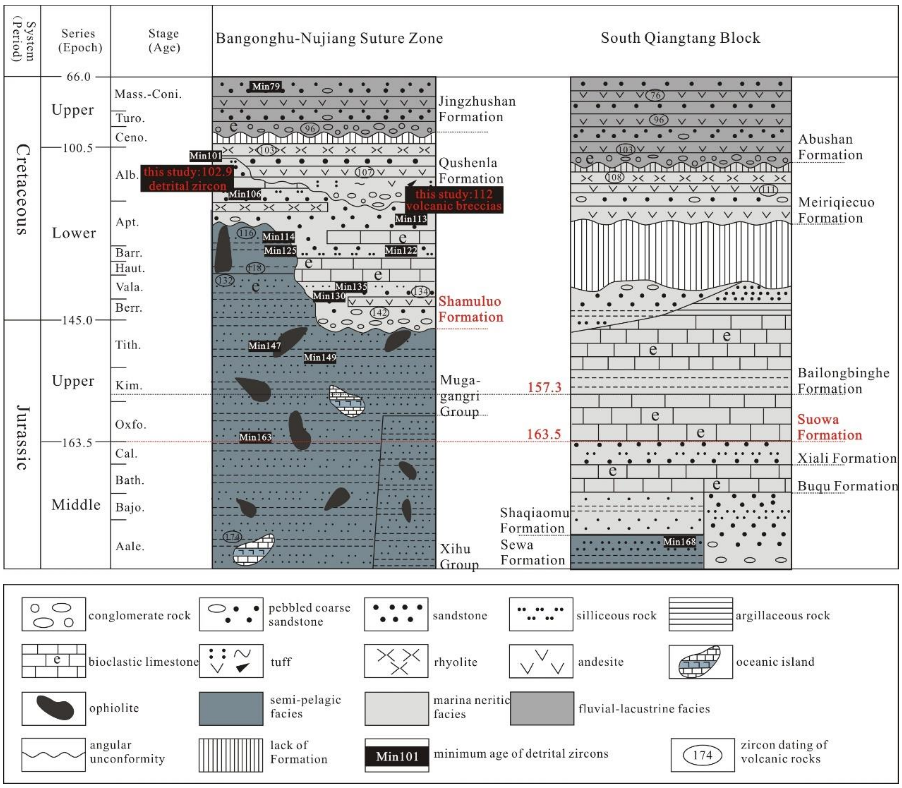

Figure 12. Comparison of stratigraphic ages between the central part of the Bangong Co-Nujiang suture zone and the South Qiangtang Block (revised from Hu et al., 2022).

5.2 Analysis of provenance area

The magmatic rocks (137-108 Ma) from Early Cretaceous of the South Lhasa Terrane indicate its association with the northward subduction of the Bangong Co-Nujiang Tethys Ocean (Wu et al. 2016). The zircon age of the Shamuluo Formation in the study area is consistent with it, but considering the large transportation distance of the provenance, we believe that this is a magmatic event of different property under the background of northward subduction of the Bangong Co-Nujiang Tethys Ocean, representing the low-angle subduction of the oceanic basin and the arc-trench system respectively. Therefore, the author does not agree with the possibility of the South Lhasa Terrane as the provenance of the Shamuluo Formation. The diagenetic age of the magmatic rocks from Late Jurassic in the Middle Lhasa Block is concentrated in 140-160 Ma (Yan et al. 2017), only Zhu et al. (2011a) obtained the age of volcanic rocks in the Zenong Group at 129-131 Ma, which is consistent with the age of some zircon grains obtained from the sampling point JS01-04. Magmatic rocks in the Early Cretaceous include diorite granite, monzogranite and quartz diorite, and the ages are mainly concentrated in 110Ma (Zhu et al. 2009a), 113-134 Ma (Zhu et al. 2009a) and

https://doi.org/10.5194/egusphere-2022-631
Preprint. Discussion started: 25 July 2022

110-133 Ma (Booth et al. 2004; Chiu et al. 2009), which is completely consistent with the stratigraphic age of the Shamuluo Formation in the suture zone. While the weak peraluminous I-type granites (134-127 Ma) (Zhu et al. 2016), the strong peraluminous S-type acidic magmatic rocks (125-120 Ma) (Sun et al. 2015a; Zhu et al. 2016), potassium calc-alkaline basalt and andesite (131-116Ma) in the eastern part of the North Lhasa Terrane (Figure 13), these magmatic rocks range in age from 137-116 Ma, which is also consistent with the age of clastic rocks sampled JS04-01. Magmatic rocks in the age range of 116-100 Ma, including A2-type granites (116-110 Ma) (Chen et al. 2014), bimodal high-potassium basalts and rhyolites, adakitic quartz diorites (110 ± 2 Ma) (Sui et al. 2013) and low-potassium adakitic granodiorite (105-104 Ma) (Wu et al. 2015), are consistent with the age of the magmatic rock sampled JS05.The consistency of the magmatic rock age of the North Lhasa Block with the Shamuluo Formation may be caused by the two-way subduction process of the Bangong Co-Nujiang Tethys Ocean, which lead to the trench-island arc magmatic system. The consistent age of the Central Lhasa Block may suggest that there are still small immature oceanic basins in the central and northern Lhasa Blocks. During the southward subduction of the Bangong Co-Nujiang Oceanic Basin, a magmatic event occurred under the background of the back-arc collision between the small ocean basin and the Central Lhasa Block. This speculation was also confirmed by paleomagnetic data (Bian et al. 2017) and isotopic analysis of high-potassium alkaline basalts, A2-type felsic rocks (Qu et al. 2012; Chen et al. 2014). The zircon ages of the magmatic rocks in the northern and central Lhasa Blocks are highly consistent with the clastic rocks in the Shamuluo Formation, indicating that they are the potential provenance areas of the Shamuluo Formation.

Collision-related magmatic rocks in the southern margin of Qiangtang include trachyandesite at 99 Ma from the Late Cretaceous (Liu et al. 2018), bimodal volcanic rock at 97-87 Ma (Liu et al. 2018), high-magnesium andesite at 90-80 Ma (Li et al. 2017; Liu et al. 2018) and high-Mg, high-Sr and Y andesite at 95 Ma (He et al. 2018), the age of which is consistent with the volcanic rock sampled JS05 of the Shamuluo Formation, indicating that the subduction of the Bangong Co-Nujiang Oceanic Basin and the South Qiangtang Block was still in progress during this period. Calc-alkaline I-type granites aged 125-110 Ma in the Early Cretaceous (Li et al. 2014), and bimodal volcanic rocks of 113-108 Ma (Wei et al. 2017) (Figure 13) are the same age as detrital zircon grains sampled JS01-04. The zircon age of the clastic rock of the Shamuluo Formation is consistent with that of the magmatic rock, and at the same time, it is consistent with the age of the magmatic rock in the southern margin of the Qiangtang, indicating that the South Qiangtang Basin may also be the source area of clastic sandstone of the Shamuluo Formation.

https://doi.org/10.5194/egusphere-2022-631
Preprint. Discussion started: 25 July 2022

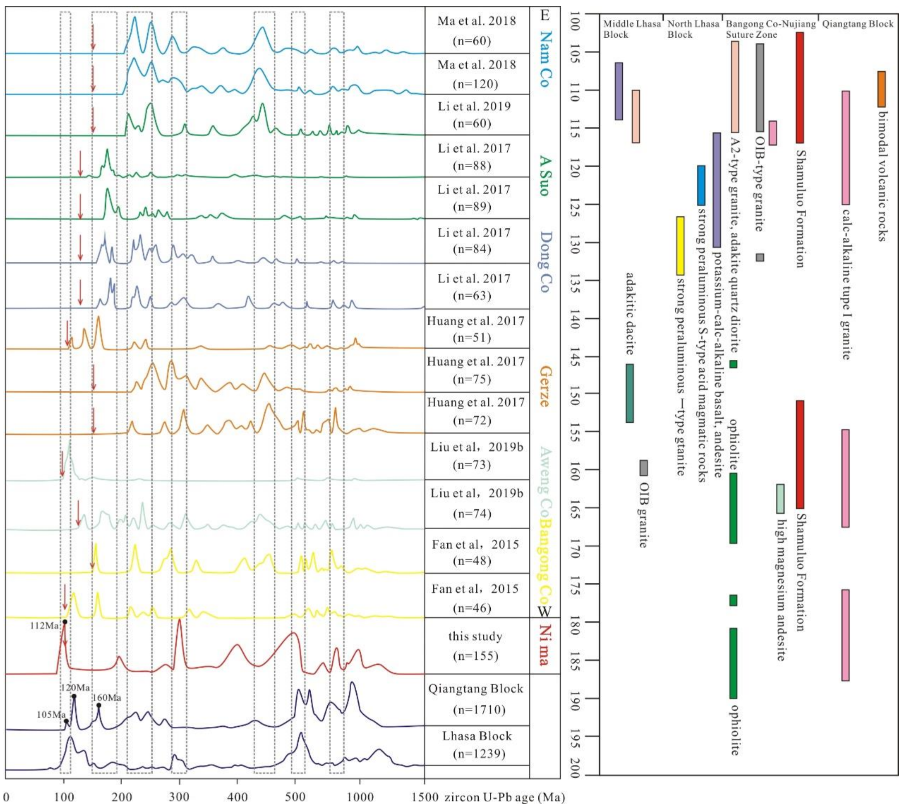

Figure 13. Age comparison of detrital zircon between Shamuluo Formation and Lhasa block and Qiangtang block, and the distribution of related magmatic rocks. Detrital zircon data is from Fan et al., (2015) and lithology distribution modified after Li et al., (2016).

The provenance area of the clastic rocks of the Shamuluo Formation has multiple possibilities, which may come from the Lhasa Block, the South Qiangtang Block and the interior of the oceanic basin. The minimum axis (K3) of the sandstone magnetic susceptibility ellipsoid of the Shamuluo Formation is perpendicular to the layer, and it is concentrated in the center of the circle to show the primary sedimentary fabric. The direction of the water flow represented by the maximum axis (K1) is mainly in the NW direction, and transitions to the SW direction and the WS direction. The paleocurrent in NW direction indicates that the provenance comes from the interior of the Lhasa Block, and the paleocurrent in SW direction indicates that the provenance may have come from the interior of the island arc. The paleocurrent in WS direction indicates that the provenance area may be in the interior of the South Qiangtang Block or on the edge of the continental shelf. At the same time, the transition of the paleocurrent direction from west to south may be the reason of landform change, which is caused by the uplift or denudation of the terrane under the collision of oceans and continents, or by the rotation of the micro-continent during the tectonic evolution. The paleocurrent of the Suowa

https://doi.org/10.5194/egusphere-2022-631
Preprint. Discussion started: 25 July 2022

Formation is mainly in the NW direction, and there is also a palaeocurrent in the ES direction. The two opposite directions of paleocurrent indicate that the provenance of sandstone in the Suowa Formation may come from the central uplift of the Qiangtang Basin or the southern suture zone and the Lhasa Block. The rose diagram (Figure 14) shows that the provenance is more from the south (suture zone or Lhasa Block), which indicates to a greater extent that the subduction of the Bangong Co-Nujiang Oceanic Basin has led to a great reduction in the area of the central ocean basin. The deep-sea shelf is transformed into a shallow-sea shelf or littoral-neritic environment, and the depositional environment and transport distance allow for the transfer of provenance, thus confirming the previous study named "scissor collision".

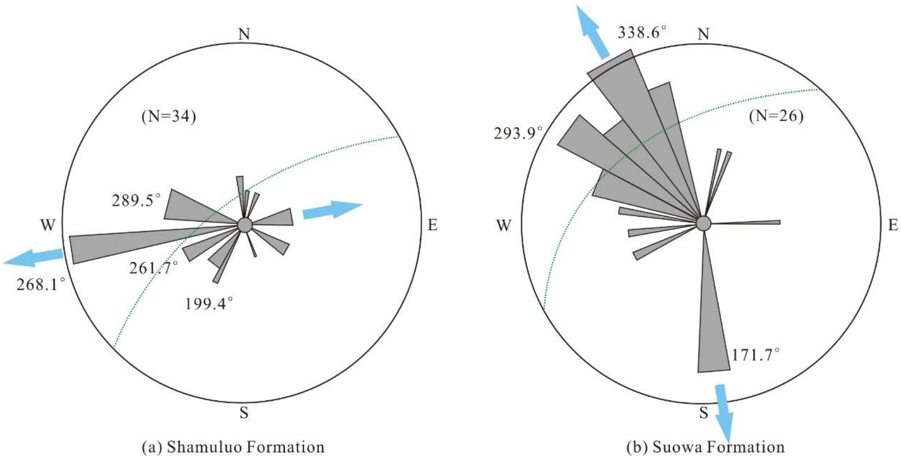

Figure 14. The rose diagram of K1 main axis distribution during stratigraphic depositional period. N represents the number of samples, and the dotted line represents the occurrence direction of the formation.

5.3 Formation reason of magnetic fabric

Previous studies on the magnetic fabric of sedimentary rocks have shown that under the action of a single stress, when the parallel layers of the sedimentary rocks are shortened by horizontal compressive stress, the magnetic fabric will undergo coaxial deformation and progressive evolution with the increase of strain. The sedimentary fabric was transformed into five strain fabrics (Ramsay and Huber 1983; Pares et al. 1999; Saint-Bezar et al. 2002; Luo et al. 2009). In sedimentary-related fabrics, gravity and hydrodynamic environment are the main controlling factors. There are two main manifestations of magnetic lineation and paleocurrent: the medium velocity is low, and the maximum axis (K1) of the magnetic susceptibility ellipsoid is consistent with the direction of paleocurrent; when the medium velocity is high, K1 is perpendicular to the direction of the paleocurrent (Ress and Woodall 1975; Borradaile and Henry 1997; Soto et al. 2009). The stress magnetic fabric caused by the tectonic deformation is the secondary superposition of the tectonic deformation on the primary sedimentary fabric, and the corresponding tectonic events can be obtained by analyzing the stress direction

https://doi.org/10.5194/egusphere-2022-631
Preprint. Discussion started: 25 July 2022

of the K1 axis (Figure 15).

The magnetic susceptibility anisotropy of the sandstone samples from the Shamuluo Formation shows that the K3 axis is perpendicular to the layer, and the K1 axis is randomly arranged without showing a preferred direction. It is a manifestation of paramagnetic minerals (various layered silicates: chlorite and clay minerals) (He et al. 2022) in hydrostatic environments parallel to the layers of sedimentary rocks. The K3 axis of some sandstone samples in the Suowa Formation is slightly deviated from the center of the ellipsoid, and the K1 axis is in the preferred direction, showing the orientation of the magnetic mineral particles with the direction of the water flow. And the direction of the paleocurrent reflected by the K1 axis is fixed in the fan-shaped area, which is the direction of the paleocurrent in the weak current environment. The tectonic stress-deformed magnetic fabric is reflected in limestone and sandstone of three sampling points in the Suowa Formation. The morphological distribution of K1 and K3 axes of the magnetic susceptibility ellipsoid of limestone in the Suowa Formation is consistent with the pencil-like magnetic fabric defined by the predecessors (Figure 15). However, the magnetic lineation of points 1 and 3 are distributed along the NE-SW direction, and the magnetic lineation of point 2 are arranged along the NW-SE direction. There are two situations for the trend of magnetic lineation in the stress environment: In the background of extrusion, the magnetic lineation is perpendicular to the maximum principal stress and parallel to the direction of strata (Cifelli et al. 2009; Soto et al. 2016); in a tensile setting, the magnetic lineation is parallel to the minimum principal stress (Faccenna et al. 2002). According to the different distribution patterns of the two magnetic lineation, it is rare that there are tectonic events of two perpendicular stress in the same diagenetic stage. And the principal stress directions of the tectonic movement in the Qiangtang Block during the Indosinian period were SN and NE-SW directions (He and Zheng 2016). Therefore, we believe that no matter what the stress direction is, the limestone of Suowa Formation reflects the extensional or compressional tectonic background related to the subduction of the oceanic basin, and there must be a conversion between the compressional background and the extensional background. The sandstones of the three sampling points in the Suowa Formation show a tensile lineation fabric, the maximum axis (K1) of the magnetic susceptibility ellipsoid is perpendicular to the bedding, and the foliation is basically not developed, and the tensile lineation (K1) is NE-SW trending (Figure 16). To a large extent, the existence of the tensile lineation fabric indicates that the thrust fault is caused by the strong compressional deformation in NE-SW direction, which is led to the vertical deformation of the stratum. The direction of the tectonic stress reflected by the tensile lineation is consistent with the stress direction of the limestone in the Suowa Formation. The two together indicate that the South Qiangtang Basin is subject to the compressive stress in NE-SW direction. And sampling points 1 and 3 of limestone should be tensile background, sampling point 2 of limestone should be compressive background. This indicates that the Bangong Co-Nujiang Tethys Oceanic Basin had subduction movements in opposite directions in the Suowa Formation of Late Jurassic.

https://doi.org/10.5194/egusphere-2022-631
Preprint. Discussion started: 25 July 2022

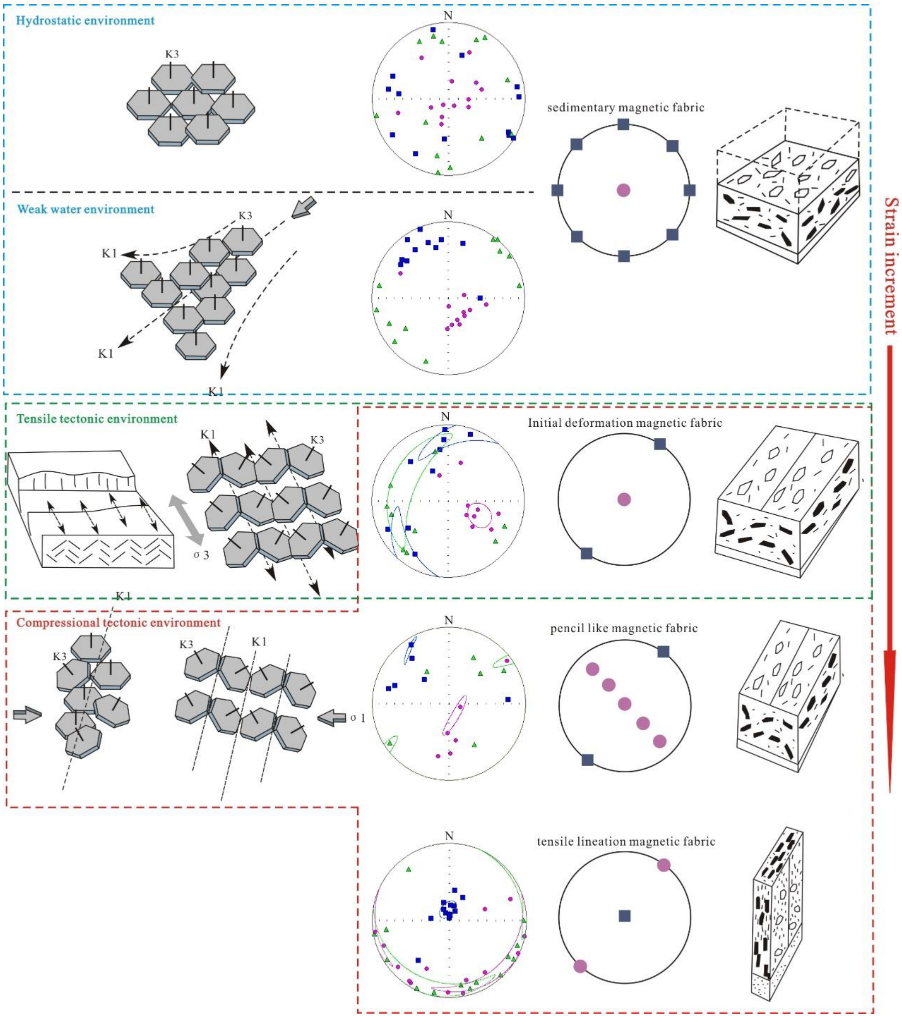

Figure 15. Causes of magnetic fabric and their increasing strain states in different depositional and tectonic environments (modified after He et al., 2022).

https://doi.org/10.5194/egusphere-2022-631
Preprint. Discussion started: 25 July 2022

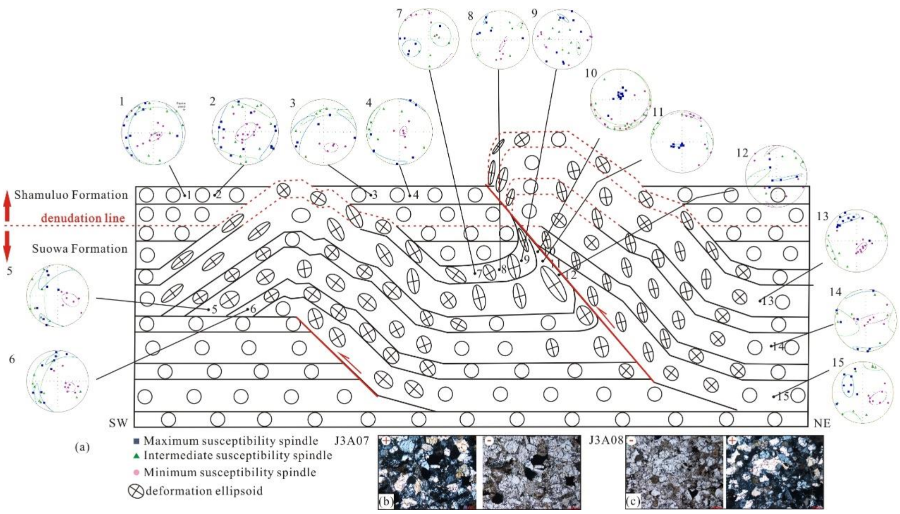

Figure 16. Characteristics of sedimentary fabric and strain fabric, and their formation causes. (a) the performance of different magnetic fabrics under correlated fold structures; (b) (c) mineral fracturing under magnetic fabrics of tensile lineation and weakly cleavage. The red dotted line indicates erosion. The Lower Suowa Formation was denuded and the Upper Shamuluo Formation was deposited. Magnetic fabric meaning: 1-4, sedimentary fabric of Shamuluo Formation; 5-6, initial deformation magnetic fabric; 7-9, pencil like magnetic fabric; 10-12, tensile lineation magnetic fabric; 13-15, sedimentary fabric of Suowa Formation.

In addition, 10 sandstone samples from the Shamuluo Formation and 9 sandstone samples from the Suowa Formation were subjected to statistics of thin-section particle, and the statistical results were projected to Dickison triangle diagram (Dickinson et al. 2009) of Q-F-L (quartz-feldspar-lithic) and Qm-F-L (monolithic quartz-feldspar-lithic). The triangular diagram shows that the Shamuluo Formation falls into a cutting arc environment and the Suowa Formation falls into a cyclic orogenic environment (Figure 17). The environment of cutting island-arc indicates that the tectonic environment has been denuded for a long time, corresponding to the migration of the paleocurrent to the provenance by the stable sedimentary fabric. Cyclic orogenic belts indicate that the provenance comes from fold-thrust belts, which correspond to thrust faults in the context of strike-slip basins. To a large extent, it leads to the generation of stress-deformation fabrics.

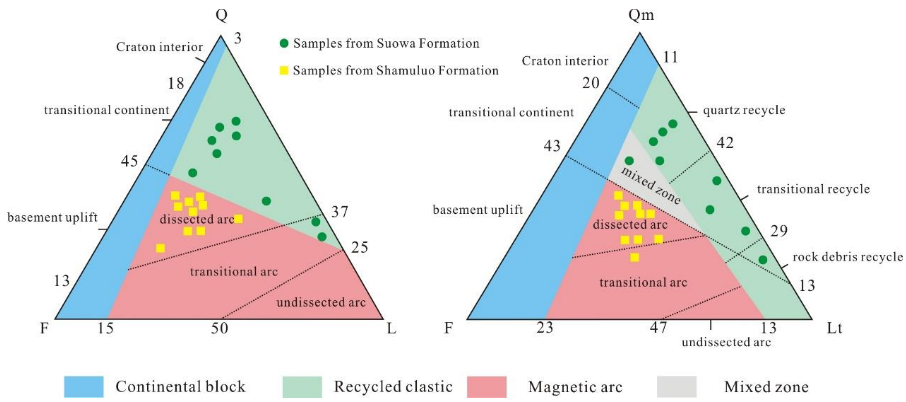

Figure 17. Analysis of geotectonic background by Q-F-L and Qm-F-Lt triangular diagram (base map from Dickinson et al., 2009).

5.4 The tectonic significance of oceanic basin subduction

5.4.1 Subduction-combination time of Bangong Co-Nujiang Tethys Oceanic Basin

The views of "through-time closure" and "scissor collision" on the Bangong Co-Nujiang Tethys Ocean are derived from studies on the ages of basalt and granite in oceanic island (Fan et al. 2015), and it is believed that the closing time from east to west is 116.6 ± 0.8 Ma, 120 ± 1.4 Ma, 107.8 ± 8.1 Ma, 96.0 ± 1.1 Ma, respectively. We agree with this point of view, and believe that at least in the middle of the Bangong Co-Nujiang suture zone, the Bangong Co-Nujiang Tethys Oceanic Basin and the Qiangtang Block are being merged and are in the late stage. In this paper, the age of the clastic rocks in the Shamuluo Formation is 112-131 Ma, the weighted average age of the magmatic rocks is 102.9 Ma, and the age of the Suowa Formation is 163.5-157.3 Ma. The study of magnetic fabric shows that the clastic rock of Shamuluo Formation belongs to sedimentary fabric, the block is relatively stable without tectonic deformation, and the block belongs to a stable period. However, the limestone and sandstone of the Suowa Formation have pencil-like and tensile lineation magnetic fabrics, all of which are caused by stress deformation, corresponding to the compressive and tensile tectonic environments of the Bangong Co-Nujiang Tethys Oceanic Basin and the South Qiangtang Block. This is in line with the subduction of Bangong Co-Nujiang Oceanic Basin to Qiangtang Block under the tectonic background. These evidences suggest that the Suowa Formation around 160 Ma was in a relatively complex tectonic environment. It corresponds to the cooling event caused by the rapid uplift of the central uplift in the Qiangtang Block due to the impact of subduction and collision (Zhao et al. 2019). Provenance studies show that the sediments of the Shamuluo Formation in the suture zone and the Suowa Formation in the South Qiangtang Block may have come from the Lhasa terrane, the Bangong Co-Nujiang suture zone or the

https://doi.org/10.5194/egusphere-2022-631
Preprint. Discussion started: 25 July 2022

Qiangtang terrane. Considering the transportation distance and transportation environment of source, only under the ideal conditions of the two can the clastic rocks be transported to each other in the two blocks. The sandstone samples of the Shamuluo Formation have detrital zircon grains and mineral grains with high roundness, which also indicate long-distance migration. If there are still deep-sea trenches or deep-sea continental shelves in the Bangong Co-Nujiang Tethys Ocean or the southern margin of Qiangtang, it is impossible to effectively connect the two blocks with such a large land gap, and it is impossible to realize the transportation of provenance. Therefore, long-distance transportation of source can only be realized in the littoral-shallow marine environment or in the terrestrial environment, which signifies the reduction of land separation. At the same time, the zircon age at 102.9 Ma of the volcanic rocks from the Shamuluo Formation also indicates that there were still tectonic thermal events occurring at this time. Therefore, the time for the end of the subduction on the central Bangong Co-Nujiang Oceanic Basin is limited to 102.9-131 Ma, which indicates that the combination between Bangong Co-Nujiang Tethys Oceanic Basin and the southern margin of Qiangtang is nearing completion.

Paleomagnetism studies the collision-joint time by comparing paleolatitude positions of the Qiangtang Block and the Lhasa Block in the Mesozoic. By comparing the paleolatitude of the Qiangtang Block (Chen et al. 2017; Meng et al. 2017; Cao et al. 2018) and the Lhasa Block (0tofuji et al. 2007; Sun et al. 2012; Tang et al. 2013; Ma et al. 2014; Yang et al. 2015a; Yi et al. 2015; Li et al. 2016; Ma et al. 2017; Tong et al. 2017; Cao et al. 2017; Li et al. 2017; Bian et al. 2017;), it indicates that the two blocks moved towards the end of the merging at 150 Ma, and achieved merging around 145 Ma. At the same time, the plate is at 20° in North Latitude (Figure 18). Combined with paleomagnetic research, it is believed that the Lhasa Block and the Qiangtang Block were combined at 145 Ma, which means the closure of the Bangong Co-Nujiang Tethys Ocean. But the continuous subduction of its remnant oceanic basin ended after 102.9-131 Ma.

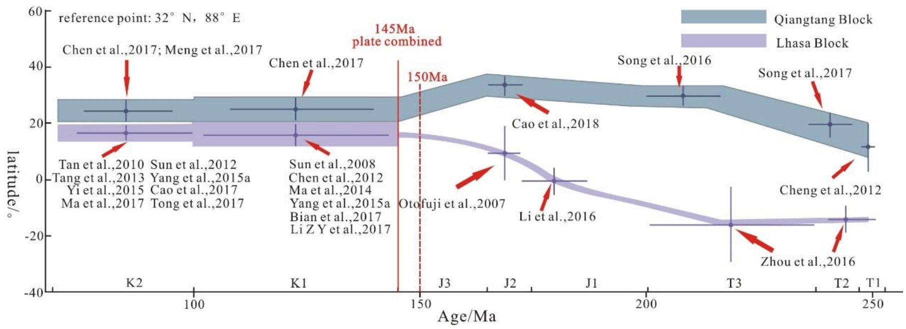

Figure 18. Paleolatitude changes and time of combination between the Lhasa and Qiangtang Blocks since the Triassic.

5.4.2 Subduction polarity of Bangong Co-Nujiang Tethys Oceanic Basin

https://doi.org/10.5194/egusphere-2022-631
Preprint. Discussion started: 25 July 2022

Although predecessors have various views on the subduction polarity of the Bannu Oceanic Basin, the author is more inclined to the view that the upwelling of the asthenosphere caused by the slab rotation to the slab separation, which lead to the change of subduction polarity by the ocean basin. (Gvirtzman and Nur 1999; Conrad and Lithgow-Bertelloni 2002; Tatsumi 2006; Grove et al. 2009;). During the period from the Late Jurassic to the Early Cretaceous, due to the enhanced northward subduction of the Yarlung Zangbo River, the southward subduction of the Bannu Ocean was hindered (Ji et al. 2009; Pan et al. 2012). With the reentry and break-off of the subducting plate under the oceanic basin, the asthenosphere upwelled, and the Bannu Oceanic Basin gradually transformed into a northward subduction. Bidirectional subduction triggered a series of magmatic events (Zhu et al. 2009, 2011, 2013; Sui et al. 2013), including the fore-arc basin of Biluo Co in the South Qiangtang Basin (Ma et al. 2017) and the Lalong ophiolite. The evolution of the Bangong Co-Nujiang suture zone and the Shiquan River-Nam Co-Bomi suture zone is also the result of the complete closure of the corresponding ocean basins under the action of the horizontal compression in NS direction. The Oxford period corresponding to 163.5-157.3 Ma of the Suowa Formation in the Qiangtang Block is the period of global sea level fall, but the Oxford period in the Qiangtang Basin shows regional sea level rise. The regional sea level rise is due to the fact that the rate of regional subsidence is greater than the rate of global sea level fall under the tectonic background of Qiangtang extension, which indicates that the Bannu Oceanic Basin is subducting southward at this time.

Cawood et al. (2012) proposed that the difference between the crystallization age of detrital zircon and the age of the sedimentary strata can reflect the different tectonic settings of the sedimentary basin where the detrital zircon is located. According to the lag time difference of rock masses under different tectonic backgrounds, the tectonic backgrounds are divided into three categories: (1) the age of the detrital zircon in the fore-arc basin and the trench basin is similar to the age of the sedimentary strata under the convergence background; (2) the crystallization age of detrital zircon in the collision background (50%-10%) is close to the depositional age (100Ma<lag time<150Ma); (3) the lag time of detrital zircon is the largest in the extensional background, and only less than 5% of the zircon particles have a lag time of less than 150 Ma. Based on this, we believe that the main body of detrital zircon grains from the Shamuluo Formation is in the collision tectonic background, and a few are in the convergence background, and the convergence background occurs before the collision background (Figure 19). The generation of the convergence background is related to the tectonic process of the northward subduction of the Bannu Oceanic Basin to the South Qiangtang Block, until the oceanic basin completes its subduction and reduction. Then the suture zone collided with the back-arc basin of the South Qiangtang Block, resulting in a collision tectonic environment. Combined with the causes of the pencil-like tectonic stress on limestone from the Suowa Formation in the Qiangtang Block, this paper believes that the Bannu Oceanic Basin was in the process of northward subduction during the deposition of the Shamuluo Formation. This is consistent with the view of south-north two-way subduction proposed by previous studies, and puts forward specific constraints on the

https://doi.org/10.5194/egusphere-2022-631
Preprint. Discussion started: 25 July 2022

polarity transition time and the completion time of the combination between the central oceanic basin and the Qiangtang Block. In the Suowa Formation (163.5-157.3 Ma) of Late Jurassic, the subduction polarity of the Bannu Oceanic Basin changed, from southward to northward. The Bangong Co-Nujiang Tethys Ocean was closed at 145 Ma, and the residual oceanic basin stopped subduction after 131-102.9 Ma.

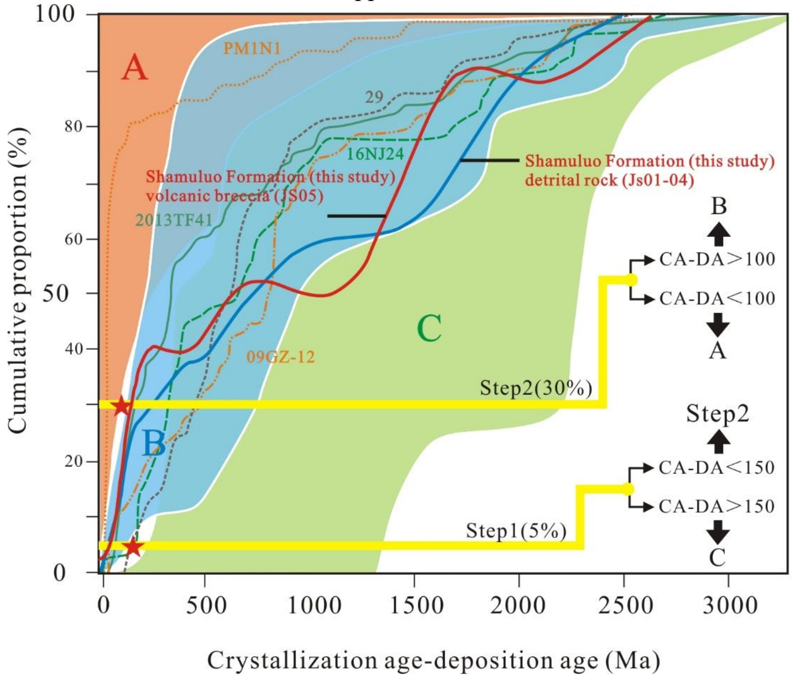

Figure 19. Difference of crystallization age and depositional age in different tectonic backgrounds of the Shamuluo Formation in the Bangong Co-Nujiang suture zone. General fields for convergent (A), collisional (B), and extensional (C) basins are from Cawood et al., (2012). The CA is represented by the measured U-Pb age of individual zircons, while the DA is represented by the youngest detrital zircon age of each sample. Other data source is from Fan et al., (2015).

6. Conclusions

For the Shamuluo Formation from the Bangong Co-Nujiang Suture Zone and the Suowa Formation from the South Qiangtang Block, we have obtained the following conclusions by comprehensively studying the petromineralogy, geochronology and magnetic fabric:

(1) The zircon grains of sandstone in the Shamuluo Formation are short columnar and elliptical, which are related to long-distance migration. The zircon grains of the pyroclastic rocks in the Shamuluo Formation are long columnar, and a few grains are metamorphic and recrystallized in a white acyclic structure, and most of them

https://doi.org/10.5194/egusphere-2022-631
Preprint. Discussion started: 25 July 2022

have oscillating rings related to magmatic origin. The weighted average age of the pyroclastic rocks is 102.9 Ma, and the sandstone age mainly has 4 peaks, with the largest number of particles at 100-300 Ma. The provenance area of sandstone in the Shamuluo Formation is a magmatic arc, which may also come from the Qiangtang Block; the provenance area of the sandstone in the Suowa Formation is a cyclic orogenic belt, and it may also come from the northern margin of the Lhasa Block.

(2) The magnetic minerals in the clastic rocks of the Shamuluo and Suowa Formations are mainly magnetite. The sandstone of the Suowa Formation is low-coercivity minerals, the sandstone of the Shamuluo Formation and the limestone of the Suowa Formation are high-coercivity minerals. The magnetic fabric of the Shamuluo Formation is sedimentary fabric, which is related to the paleocurrent; most of the sandstones and limestones of the Suowa Formation are strain fabrics, which correspond to the geological background of subduction on oceanic basin, and a few are sedimentary fabrics in a weak current environment. The sedimentary fabric can reflect the direction of the provenance area, while the deformation fabric reflects the tectonic setting of extrusion and extension.

(3) The age of the Suowa Formation is Late Jurassic (163.5-157.3 Ma), and the age of the Shamuluo Formation is later than that of the Suowa Formation, belonging to the Early Cretaceous (131-102.9 Ma). The Bangong Co-Nujiang Tethys Oceanic Basin has been subducting southward continuously since the Jurassic. Affected by the northward subduction of the Yarlung Zangbo Tethys Ocean and the separation of the slab, the upwelling of the asthenosphere caused the oceanic basin to begin its northward subduction. The switching time of subduction polarity was at 163.5-157.3 Ma, the Bangong Co-Nujiang Tethys Ocean was closed at 145 Ma, and the central residual oceanic basin completed a continuous northward subduction at 131-102.9 Ma, which verified the “scissor collision” proposed by the predecessors.

https://doi.org/10.5194/egusphere-2022-631
Preprint. Discussion started: 25 July 2022

References

Ao, H., and Deng, C.L. 2007. Review in the identification of magnetic minerals, PROGRESS IN GEOPHYSICS, v. 22, no. 2, p. p. 432-442. doi:10.3969/j.ssn.1004-2903.2007.02.015.

Bian, W.W., Yang, T.S., Ma, Y.M., Jin, J.J., Gao, F., Zhang, S.H., Wu, H.C., and Li, H.Y. 2017. New Early Cretaceous palaeomagnetic and geochronological results from the far western Lhasa terrane: Contributions to the Lhasa-Qiangtang collision, Scientific Reports, v. 16216. doi:org/10.1038/s41598-017-16482-3.

Booth, A.L., Zeitler, P.K., Kidd, W.S.F., Wooden, J., Liu, Y.P., Idleman, B., Hren, M. and Chamberlain, C.P. 2004. U-Pb zircon constraints on the tectonic evolution of southeastern Tibet, Namche Barwa area, American Journal of Science, v. 304, no. 10, p. p. 889-929.

Borradaile, G.J., and Henry, B. 1997. Tectonic applications of magnetic susceptibility and its anisotropy, Earth-Science Reviews, v. 42, no. 1-2, p. p.49-93. doi:10.1016/S0012-8252(96)00044-X.

Cao, Y., Sun, Z.M., Li, H.B., Pei, J.L., Liu, D.L., Zhang, L., Ye, X.Z., Zheng, Y., He, X.L., GE, C.L., and Jiang, W. 2018. New paleo-magnetic results from Middle Jurassic limestones of the Qiangtang terrane, Tibet: Constraints on the evolution of the Bangong-Nujiang Ocean, Tectonics, v. 38, no. 1, p. p. 215-232. doi:org/10.1029/2017TC004842.

Cao, Y., Sun, Z.M., Li, H.B., Pei, J.L., Jiang, W., Xu, W., Zhao, L.S., Wang, L.Z., Li, C.L., Ye, X.Z., and Zhang, L. 2017. New Late Cretaceous paleomagnetic data from volcanic rocks and red beds from the Lhasa terrane and its implications for the paleolatitude of the southern margin of Asia prior to the collision with India, Gondwana Research, v. 41, p. p. 337-351. doi:org/10.1016/j.gr.2015.11.006.

Cawood, P.A., Hawkesworth, C.J., and Dhuime, B. 2012. Detrital zircon record and tectonic setting, Geology, v. 40, no. 10, p. p. 875-878. doi:org/10.1130/G32945.1.

Cifelli, F., Ballato, P., Alimohammadian, H., Sabour, J. and Mattei, M. 2015. Tectonic magnetic lineation and oroclinal bending of the Alborz range: Implications on the Iran-Southern Caspian geodynamics, Tectonics, v. 34, no. 1, p. p. 116-132. doi:10.1002/2014tc003626.

Cifelli, F., Mattei, M., Chadima, M., Lenser, S., and Hirt, A.M. 2009. The Magnetic fabric in “underformed clays”: AMS and neutron texture analyses from the Rif Chain (Morocco), Tectonophysics, v. 466, no. 1-2, p. p. 79-88. doi:org/10.1016/j.tecto.2008.08.008.

Chen, S.S., Fan, W.M., Shi, R.D., Xu, J.F., Yang, K., and Pan, Z. 2021. Cretaceous volcanic rocks in Yunzhug area, Central Tibet, China, associated with arc-continent collision in the Tibetan Plateau, Lithos, v. 80, no. 10587. doi:ogr/10.1016/j.lithos.2020.105827.

Chiu, H.Y., Chuang, S.L., Wu, Y.F., Liu, D.Y., Liang, Y.H., Lin, I.j., lizuka, Y., Xie, L.W., Wang, Y.B., and Chu, M.F. 2009. Zircon U-Pb and Hf isotopic constraints from eastern Malayanmalayan batholiths on the precollisional magmatic and tectonic

https://doi.org/10.5194/egusphere-2022-631
Preprint. Discussion started: 25 July 2022

evolution in southern Tibet, Tectonophysics, v. 477, no. 1-2, p. p. 3-19. doi:org/10.1016/j.tecto.2009.02.034.

Chen, Y., Zhu, D.C., Zhao, Z.D., Meng, F.Y., Wang, Q., Santosh, M, Wang, L.Q., Dong, G.C., and Mo, X.X. 2014. Slab breakoff triggered ca. 113Ma magmatism around Xainza area of the Lhasa Terrane, Tibet. Gondwana Research, v. 26, no. 2, p. p. 449-463. doi:org/10.1016/j.gr.2013.06.005.

Chen, W., Zhang, S., Ding, J., Zhang, J., Zhao, X., Zhu, L., Yang, W., Yang, T., Li, H., and Wu, H. 2017. Combined paleo-magnetic and geochronological study on Cretaceous strata of the Qiangtang terrane, central Tibet, Gondwana Research, v. 41, p. p. 93-109. doi:org/10.1016/j.gr.2015.07.004.

Conrad, C.P., and Lithgow-Bertelloni, C. 2002. How mantle slabs drive plate tectonics, Science, v. 298, no. 5591, p. p. 207-209. doi:10.1126/science.1074161.

Dickinson, W.R., and Gehrels, G.E. 2009. Use of U-Pb ages of detrital zircons to infer maximum depositional ages of strata: A test against a Colorado Plateau Mesozoic database, Earth and Planetary Sciences Letters, v. 288, p. p. 115-125. doi:org/10.1016/j.epsl.2009.09.013.

Fan, J.J., Li, C., Xie, C.M., Wang, M., and Chen, J.W. 2015. The Evolution of the Bangong-Nujiang Neo-Tethys Ocean: Evidence from Zircon U-Pb and Lu-Hf Isotopic Analyses of Early Cretaceous Oceanic Islands and Ophiolites, Tectonphysics, v. 655, p. p. 27-40. doi:org/10.1016/j.tecto.2015.04.019.

Faccenna, C., Speranza, F., Caracciolo, F.D., Mattei, M. and Oggiano, G. 2002. Extensional tectonics on Sardinia (Italy): insights into the arc-back-arc transitional regime, Tectonophysics, v. 365, no. 4, p. p. 213-232. doi:org/10.1016/S0040-1951(02)00287-1.

Fu, X.G., Wang, J., Wen, H.G., Song, C.Y., Wang, Z.W., Zeng, S.Q., Feng, X.L., and Wei, H.Y. A Toarcian Ocean Anoxic Event record from an open-ocean setting in the eastern Tethys: Implications for global climatic change and regional environmental perturbation, Science China Earth Sciences, v. 64, no. 11, p. p. 1860-1872. doi:org/10.1007/s11430-029-9753-1.

Gurioli, L., Pareschi, M.T., Zanella, E., Lanza, R., Deluca, E., and Bisson, M. 2005. Interaction pyroclastic density currents with human settlements: Evidence from ancient Pompeii, Geology, v. 33, no. 6, p. p. 441-444. doi:10.1130/g21294.1.

Guynn, J., Kapp, P., Pullen, A., Heizler, M., Gehrels, G., and Ding, L. 2006. Tibetan basement rocks near Amdo reveal “missing”Mesozoic tectonism along the Bangong suture, central Tibet, Geology, v. 34, no. 6, p. p. 505-508. doi:org/10.1130/G22453.1.

Gvirtzman, Z., and Nur, A. 1999. The formation of Mount Etna as the consequence of slab rollback, Nature, v. 401, no. 6755, p. p. 782-785. doi:org/10.1038/44555.

Grove, T.L., Till, C.B., Lev, E., Chatterjee, N., and Medard, E. 2009. Kinematic variables and water transport control the formation and location of arc volcanoes, Nature, v. 459, no. 7247, p. p. 694-697. doi:org/10.1038/nature08044.

Gao, X.L., Li, J.H., and Liu, P. 2022. Analysis of magnetic fabric characteristics of Xiashagou section and the environment changes of ancient lakes in Nihewan Basin, Quaternary Sciences, v. 42, no. 2, p. p. 562-576. doi:10.11928/j.issn.1001-7410.2022.02.19.

Hu, P.Y., Zhai, Q.C., Jahn, B.M., Wang, J., Li, C., Chung, S.L., Lee, H.Y., and Tang, S.H. 2017. Late Early Cretaceous magmatic rocks(118-113Ma) in the middle segment of the Bangong-Nujiang suture zone, Tibetan Plateau: Evidence of lithospheric delamination, Gondwana Research, v. 44, p. p. 116-138. doi:org/10.1016/j.gr.2016.12.005.

Hu, X.M., Ma, A.L., Xue, W.W., Garzanti, E., Cao, Y., Li, S.M., Sun, G.Y., and Lai, W. 2022. Exploring a lost ocean in the Tibetan Plateau: Birth, growth, and demise of the Bangong-Nujiang Ocean, Earth-Science Reviews, v. 229. doi:org/10.1016/j.earscirev.2022.104031.

Hermann, J., Rubatto, D., Korsakov, A., and Shatsky, V.S. 2001. Multiple Zircon Growth During Fast Exhumation of Diamondiferous, Deeply Subducted Continental Crust (Kokchetav Massif, Kazakhstan), Contribution to Mineralogy and Petrology, v. 141, no. 1, p. p. 66-82. doi:org/10.1007/s004100000218.

Hroudam, F. 1994. A technique for the measurement of thermal changes of magnetic susceptibility of weakly magnetic rocks by the CS-2 apparatus and KLY-2 Kappabridge, Geophysical Journal Internation, v. 118, no. 3, p. p. 604-612. doi: 10.1111/j.1365-246X.1994.tb03987.x.

Huang, T.T., Xu, J.F., Chen, J.L., Wu, J.B., and Zeng, Y.C. 2017. Sedimentary record of Jurassic Northward subduction of the Bangong-Nujiang Ocean: Insights from detrital zircons, International Geology Review, v. 59, no. 2, p. p. 166-184. doi:org/10.1080/00206814.2016.1218801.

He, H., Li, Y., Wang, C., Zhou, A., Qian, X.Y., Zhang, J.W., Du, L.T. and Bi, W.J. 2018. Late Cretaceous (ca. 95Ma) magnesian andesites in the Biluoco area, southern Qiangtang subterrane, central Tibet: Petrogenetic and tectonic implications, Lithos, no.302-303, p. p. 389-404. doi:org/10.1016/j.lithos.2018.01.013.

He, X., Shen, Q., Jiang, K., Li, C.Z, Wu, G.Z., Ran, Y.Z., Jin, C.S., and Liang, W.T. 2022. Room and low temperature magnetic fabrics of fine-grained clastic rocks: A case study of the Cretaceous Huicheng basin, Qingling orogen, Chines Journal of Geophysics, v. 65, no. 2, p. p. 737-753. doi:10.6038/cjp2022P0202.

He, B.Z., and Zheng, M.L. 2016. Structal characteristic and formations dynamics: A review of the main sedimentary basins in the contient of China, Acta Geological Sinica. v. 904, p. p. 1156-1194.

Ishizuka, O., Tani, K., Reagan, M.K. 2014. Izu-Bonia-Mariana Forearc Crust as a Modern Ophiolite Analogue, Elements, v. 10, no. 2, p. p. 115-120. doi:org/10.2113/gselements.10.2.115.

Ji, W.Q., Wu, F.Y., Chung, S.L., Li, J.X., and Liu, C.Z. 2009. Zircon U-Pb geochronology and Hf isotopic constraints on petrogenesis of the Gangdese batholith, southern Tibet, Chemical Geology, v. 262, no. 3-4, p. p. 229-245. doi:org/10.1016/j.chemgeo.2009.01.020.

Kapp, P., Decelles, P.G., Gehrels, G.E., Heizler, M., and Ding, L. 2007. Geological records of the Lhasa-Qiangtang and Indo-Asian collisions in the Nima area of Central Tibet, Geological Society on America Bulletin, v. 119, no. 7-8, p. p. 917-933. doi:org/10.1130/B26033.1.

Kong, Y.F., Sun, L., Shen, Z.S., Ge, J.Y. and Deng, C.L. 2018. Anisotropy of magnetic susceptibility of the Neogene Guonigou section in the Linxia Basin and its paleoenvironmental significance, Chinese Journal of Geophysics. v. 61, no. 11, p. p. 4518-4529. doi:10.6038/cjg2018M0245.

Liu, D.L., Huang, Q.S., Fan, S.Q., Zhang, L.Y., Shi, R.D., and Ding, L. 2014. Subduction of the Bangong-Nujiang Ocean: constraints from granites in the Bangong Co area, Tibet, Geological Journal, v. 49, no. 2, p. p. 188-206. doi:org/10.1002/gj.2510.

Li, F.Q., Tang, J.X., Zhang, J., Song, Y., Li, H.F., Lin, B., and Wang, N. 2022. Discovery of Late Early Cretaceous diorite porphyrite from the Shamuluo Formation in the Gaize area, Tibet: Response to the northward subduction plate rollback event of Bangongco-Nujiang Tethys Ocean, Acta Petrological Sinica, v. 38, no. 1, p. p.185-208. doi:10.18654/1000-0569/2022.01.13.

Liu, Y.S., Hu, Z.C., Zong, K.Q., Gao, C.G., Gao, S., Xu, J. and Chen, H.H. 2010. Reappraisement and Refinement of Zircon U-Pb Isotope and Trace Element Analyses by LA-ICP-MS, Chinese Science Bulletin, v. 55, no. 15, p. p. 1535-1546. doi:org/10.1007/s11434-010-3052-4.

Liang, W.T., Zhang, G.W., Lu, R.K., Pei, X.Z. and Jin, C.S. 2009. Magnetic fabrics study and its tectonic significance of suture zones in joint area of Qinling and Qilianshan, Chinese Journal of Geophysics, v. 52, no. 1, p. p. 140-149. doi:org/10.1002/cjg2.1329.

Li, S., Ding, L., Guilmette, C., Fu, J.J., Xu, Q., Yue, Y.H., and Henrique-Pinto, R. 2017. The Subduction-Accretion History of the Bangong-Nujiang Ocean: Constraints from Provenance and Geochronology of the Mesozoic Strata near Gaize, Central Tibet, Tectonophysics, no. 702, p. p. 42-60. doi:org/10.1016/j.tecto.2017.02.023.

Li, S.M., Zhu, D.C., Wang, Q., Zhao, Z., Zhang, L.L., Liu, S.A., Chang, Q.S., Lu, Y.H., Dai, J.G., and Zheng, Y.C. 2016. Slab-derived adakites and subslab asthenosphere-derived OIB-type rocks at 156 ± 2 Ma from the north of Gerze, central Tibet: Records of the Bangong-Nujiang oceanic ridge subduction during the Late Jurassic, Lithos, v. 262, p. p. 456-469. doi:org/10.1016/j.lithos.2016.07.029.

Liu, D.L., Shi, R.D., Ding, L., and Zou, H.B. 2018. Late Cretaceous transition from subduction to collision along the Bangong-Nujiang Tethys: New volcanic constraints from central Tibet, Lithos, no. 296-299, p. p. 452-470. doi:org/10.1016/j.lithos.2017.11.012.

Liu, W., Wu, J.L., Lei, C.Y. Wang, B., and Lang, X.H. 2019. Detrital zircon geochronology of the Shamuluo Formation in Geji region of central Tibet: Provenance and evidence for the closure time of the Bangong Co-Nujiang Tethys Ocean, Acta Petrologica Sinica, v. 35, no. 6, p. p. 1738-1756. doi:10.18654/1000-0569/2019.06.07.

Li, J.X., Qin, K.Z., Li, G.M., P. Richards, J. Zhao, J.X. and Cao, M.J. 2014. Geochronology, geochemistry, and zircon Hf isotopic compositions of Mesozoic intermediate-felsic intrusions in central Tibet: Petrogenetic and tectonic implications, Lithos, no. 198-199, p. p. 77-91. doi:org/10.1016/j.lithos.2014.03.025.

Luo, L., Jia, D., Li, H.B., Li, Y.Q., Deng, F. Chen, Z.X., Jia, Q.P., Sun, S.S., and Zhang, Y.Y. 2009. Magnetic fabric investigation in the northwestern Sichuan Basin and its

https://doi.org/10.5194/egusphere-2022-631
Preprint. Discussion started: 25 July 2022

regional inference, Physics of the Earth and Planetary Interiors, v. 173, no. 1-2, p. p. 103-114. doi:10.1016/J.PEPI.2008.11.004.

Li, Z.Y., Ding, L., Lippert, P.C., Song, P.P., Yue, Y.H., Van Hinsebergen, D.J.J. 2016. Paleomagnetic constraints on the Mesozoic drift of the Lhasa terrane (Tibet) from Gondwana to Eurasia, Geology, v. 44, no. 9, p. p. 727-730. doi:org/10.1130/G38030.1.

Li, Z.Y., Ding, L., and Song, P.P. 2017. Paleomagnetic constraints on the paleolatitude of the Lhasa block during the Early Cretaceous: Implications for the onset of India-Asia collision and latitudinal shortening estimates across Tibet and stable Asia, Gondwana Research, no. 41, p. p. 352-372.

Li, X.K., Chen, J., Wang, R.C., Li, C., Wang, M., Liu, J.H., Yu, Y.P., and Luo, A.B. 2019. Early Cretaceous tectonomagmatic evolution and basin development of western Bangong-Nujiang suture: A complete history of soft collision, Lithos, v. 344-345, p. p. 360-373. doi:org/10.1016/j.lithos.2019.06.030.

Ma, A.L., Hu, X.M., Kapp, P., Han, Z., Lai, W., and BouDagher-Fadel, M. 2018. The disappearance of the Late Jurassic Remnant Sea in the Southern Qiangtang Block (Shamuluo Formation, Najiangco Area): Implications for the Tectonic Uplift of Central Tibet, Palaeogeography, Palaeoclimatology, Palaeoecology, no. 506, p. p. 30-47. doi:org/10.1016/j. palaeo.2018.06.005.

Metcalfe, I. 2006. Palaeozoic and Mesozoic tectonic evolution and paleogeography of East Asian crustal fragments: The Korean Peninsula in context, Gondwana Research, v. 9, no. 1, p. p. 24-46. doi:org/10.1016/j.gr.2005.04.002.

Metcalfe, I. 2013. Gondwana dispersion and Asian accretion: Tectonic and palaeogeographic evolution of eastern Tethys, Journal of Asian Earth Sciences, no. 66, p. p.1-33. doi:org/10.1016/j.jsease.2012.12.020.

Meng, J., Zhao, X., Wang, C., Liu, H., Li, Y., Han, Z., Liu, T., and Wang, M. 2017. Paleomagnetism and detrital zircon U-Pb geochronology of Cretaceous redbeds from central Tibet and tectonic implications, Geological Journal, v. 53, no. 5, p. p. 2315-2533. doi:org/10.1002/gj.3070.

Ma, Y., Yang, T., Bian, W.W., Jin, J.J., Wang, Q., Zhang, S.H., Wu, H.C., Li, H.Y., Cao, L.W., Yuan, H.F., and Ding, J.K. 2017. Paleomagnetic and geochronologic results of latest Cretaceous lava flows from the Lhasa Terrane and their tectonic implications, Journal of Geophysical Research: Solid Earth, v. 122, no. 11, p. p. 8786-8809. doi:org/10.1002/2017JB014743.

Ma, Y.M., Yang, T.S., Yang, Z.Y., Zhang, S.H., Wu, H.C., Li, H.Y., Li, H.K, Chen, W.W., Zhang, J.H., and Ding, J.K. 2014. Paleomagnetism and U-Pb zircon geochronology of Lower Cretaceous lava flows from the western Lhasa terrane: New constraints on the India-Asia collision process and intracontinental deformation with Asia, Journal of Geophysical Research: Solid Earth, v. 119, no. 10, p. p. 7404-7424. doi:org/10.1002/2014JB011362.

Ma, A., Hu, X., Garzanti, E., Han, Z., and Lai, W. 2017. Sedimentary and tectonic evolution of the southern Qiangtang basin: Implications for the Lhasa-Qiangtang collision timing, Journal of Geophysical Research: Solid Earth, v. 122, no. 7, p. p. 4790-4813. doi:org/10.1002/2017JB014211.

https://doi.org/10.5194/egusphere-2022-631
Preprint. Discussion started: 25 July 2022

Otofuji, Y., Mu, C.L., Tanaka, K., Miura, D., Inokuchi, H., Kamei, R., Tamai, M., Takemoto, K., Zaman, H., and Yokoyama, M. 2007. Spatial gap between Lhasa and Qiangtang blocks inferred from Middle Jurassic to Cretaceous paleomagnetic data, Earth and Planetary Science Letters, v. 262, no. 3, p. p. 581-593. doi:org/10.1016/j.epsl.2007.08.013.

Pan, G.T., Wang, L.Q., Li, R.S., Yuan, S.H., Ji, W.H., Yin, F.G., Zhang, W.P., and Wang, B.D. 2012. Tectonic evolution of the Qinghai-Tibet Plateau, Journal of Asian Earth Sciences, no. 53, p. p. 3-14. doi:org/10.1016/j.jseaes.2011.12.018.

Pares, J.M., van der Pluijm, B.A., and Dinares-Turell, J. 1999. Evolution of magnetic fabrics during incipient deformation of mudrocks (Pyrenees, northern Spain), Tectonophysics, v. 307, no. 1-2, p. p. 1-14. doi:10.1016/S0040-1951(99)00115-8.

Qu, X.M., Wang, R.J., Xin, H.B., Jiang, J.H., and Chen, H. 2012. Age and petrogenesis of A-type granites in the middle segment of the Bangonghu-Nujiang suture, Tibetan plateau, Lithos, no. 146-147, p. p. 264-275. doi:org/10.1016/j.lithos.2012.05.006.

Ramsay, J.G., and Huber, M.I. 1983. The Techniques of Modern Structural Geology, London: Academic Press.

Ress, A.I., and Woodall, W.A. 1975. The magnetic fabric of some laboratory-deposited sediments, Earth and Planetary Science Letters, v. 25, no. 2, p. p. 121-130. doi:10.1016/0012-821X(75)90188-0.

Saint-Bezar, B., Herbert, R.L., Aubourg, C., Robion, P., Swennen, R., and Frizon de Lamotte, D. 2002. Magnetic fabric and petrographic investigation of hematite-bearing sandstones within ram-related folds: examples from the South Atlas Front (Morocco), Journal of Structural Geology, v. 24, no. 9, p. p. 1507-1520. doi:10.1016/S0191-8141(01)00140-7.

Sun, G.Y., Hu, X.M., Zhu, D.C., Hong, W.T., Wang, J.G., and Wang, Q. 2015a. Thickened juvenile lower crust-derived ~90Ma adakitic rocks in the central Lhasa terrane, Tibet, Lithos, no. 224-225, p. p. 225-239. doi:org/10.1016/j.lithos.2015.03.010.

Sui, Q.L., Wang, Q., Zhu, D.C., Zhao, Z.D., Chen, Y., Santosh, M., Hu, Z.C., Yuan, H.L., and Mo, X.X. 2013. Compositional diversity of ca. 110Ma magmatism in the northern Lhasa Terrane, Tibet: Implications for the magmatic origin and crustal growth in a continent-continent collision zone, Lithos, no. 168, p. p. 144-159. doi:org/10.1016.j.lithos.2013.01.012.

Soto, R., Larrasoana, J.C., Arlegui, L.E., Beamud, E., Oliva-Urcia, and L. Simon, J. 2009. Reliability of magnetic fabric of weakly deformed mudrocks as a palaeostress indicator in compressive settings, Journal of Structural Geology, v. 31, no. 5, p. p. 512-522. doi:10.1016/j.jsg.2009.03.006.

Soto, R., Larrasoana, J.C., Beamud, E., and Garces M. 2016. Early-Middle Miocene subtle compressional deformation in the Ebro foreland basin (northern Spain); insights from fabrics, Comptes Rendus Geoscience, v. 348, no. 3-4, p. p. 213-223. doi:org/10.1016/j.crte.2015.10.009.

Sun, Z., Pei, J., Li, H., Xu, W., Jiang, W., Zhu, Z.M., Wang, X.S., and Yang, Z.Y. 2012. Paleomagnetism of the cretaceous sediments from southern Tibet: evidence for the consistent paleolatitudes of the southern margin of Eurasia prior to the collision with

India, Gondwana Research, v. 21, no. 1, p. p. 53-63. doi:org/10.1016/j.gr.2011.08.003.

Tatsumi, Y. 2006. High-Mg andesites in the Setouchi Volcanic Belt, Southwestern Japan: analogy to Archean magmatism and continental crust formation, Annual Review of Earth and Planetary Sciences, no. 34, p. p. 467-499.

Tang, X.D., Huang, B.C., and Yang, L.K. 2013. Paleomagnetism and Ar-Ar geochronology of Cretaceous volcanic rocks in the middle Lhasa terrane, China and tectonic implications, Chinese Journal of Geophysics, v. 56, no. 1, p. p. 136-149. doi:10.6038/cjg20130114.

Tong, Y.B., Yang, Z.Y., Pei, J.L., Wang, H., Xu, Y.C., and Pu, Z.W. 2017. Paleomagnetism of the Upper Cretaceous red-beds from the eastern edge of the Lhasa Terrane: New constraints on the onset of the India-Eurasia collision and latitudinal crustal shortening in southern Eurasia, Gondwana Research, no. 48, p. p. 86-100. doi:org/10.1016/j.gr.2017.04.018.

Van Velzen, A.J., and Dekkers, A.J. 1999. The incorporation of thermal methods in mineral magnetism of loess-paleosol sequences: a brief overview, Chinese Science Bulletin, no. 44, p. p. 53-63.

Wang, B.D., Wang, L.Q., Chung, S.L., Chen, J.L., Yin, F.G., Liu, H., Li, X.B., and Chen, L.K. 2016. Evolution of the Bangong-Nujiang Tethyan ocean: insights from the geochronology and geochemistry of mafic rocks within ophiolites, Lithos, no. 245, p. p. 18-33. doi:org/10.1016/j.lithos.2015.07.016.

Wei, S.G., Tang, J.X., Song, Y., Liu, Z.B., Feng, J., and Li, Y.B. 2017. Early Cretaceous bimodal volcanism in the Duolong Cu mining district, western Tibet: Record of slab breakoff that triggered ca. 108-113Ma magmatism in the western Qiangtang terrane, Journal of Asian Earth Sciences, no. 138, p. p. 588-607. doi:org/10.1016/j.jseaes.2016.12.010.

Whattam, S.A., and Stern, R.J. 2011. The “subduction initiation rule”: a key for linking ophiolites, intra-oceanic forearcs, and subduction initiation, Contributions to Mineralogy and Petrology, v. 162, no. 5, p. p. 1031-1045. doi:org/10.1007/s00410-011-0638-z.

Wu, J.L., Liu, W., Yin, X.K., Lei, C.Y., and Wang, B. 2021. Geochronology, Zircon Hf isotope and Geochemistry of volcanic rocks from Shamuluo Formation in Western Banggongco-Nujiang Suture Zone, North Tibet, Earth Science, v. 46, no. 2, p. p. 444-459. doi:org/10.3799/dqkx.2020.104.

Wu, H., Li, C., Xu, M.J., and Li, X.K. 2015. Early Cretaceous Adakitic Magmatism in the Dachagou Area, Northern Lhasa Terrane, Tibet: Implications for Slab Roll-Back and Subsequent Slab Break-off of the Lithosphere of the Bangong-Nujiang Ocean, Journal of Asian Earth Sciences, no. 97, p. p. 51-66. doi:org/10.1016/j.jseaes.2014.10.014.

Wu, Z.H., Zhao, Z., Barosh, P.J., and Ye, P.S. 2016. Early Cretaceous tectonics and evolution of the Tibetan Plateau, Acta Geological Sinica, v. 90, no. 3, p. p. 847-857. doi:org/10.1111/1755-6724.12728.

Xie, G.G., Mo, X.H., Diao, Z.D., and Dong, G.C. 2009. Jurassic-Cretaceous sedimentation and evolution of ancient oceanic basic in Bangong Lake area, Tibet,

https://doi.org/10.5194/egusphere-2022-631
Preprint. Discussion started: 25 July 2022

Earth Science Frontiers, v. 16, no. 4, p. p. 031-039.

Xu, Y.J., Du, Y.S., Cawood, P.A., Guo, H., Huang, H., and An, Z.H. 2010. Detrital Zircon Record of Continental collison: Assembly of the Qilian Orogen, China, Sedimentary Geology, v. 230, no. 1-2, p. p. 35-45. doi:org/10.1016/j.sedgeo.2010.06.020.

Xu, Z.Q., Zhao, Z.B., Peng, M., Ma, X.X., Li, H.Q., and Zhao, J.M. 2016. Review of "orogenic plateau", Acta Petrologica Sinica, v. 32, no. 12, p. p. 3557-3571.

Xue, W.W., Ma, A.L., Hu, X.M. 2020. The redefinition of the Jurassic-Cretaceous lithostratigraphic framework in the Qiangtang Basin, Xizang Plateau, Geological Review, v. 66, no. 5, p. p. 1115-1129. doi:10.16509/j.georeview.2020.05.003.

Yan, J.J., Zhao, Z.D., Liu, D., Wang Z.Z., and Tang, Y. 2017. Geochemistry and petrogenesis of the Late Jurassic Xutu Tso batholith in central Lhasa Terrane, Tibet, Acta Petrlogica Sinica, v. 33, no. 8, p. p. 2437-2453.

Yang, T.S., Ma, Y.M., Zhang, S.H., Bian, W.W., Yang, Z.Y., Wu, H.C., Li, H.Y. Chen, W.W., and Ding, J.K. 2015a. New insights into the India-Asia collision process from Cretaceous paleomagnetic and geochronologic results in the Lhasa terrane, Gondwana Research, v. 28, no. 2, p. p. 625-641. doi:org/10.1016/j.gr.2014.06.010.

Yin, A., and Harrison, T.M. 2000. Geological evolution of the Himalayan-Tibetan Orogen, Annual Review of Earth and Planetary Sciences, no. 28, p. p. 211-280. doi:org/10.1146/annurev.earth.28.1.211.

Yi, Z.Y., Huang, B.C., Yang, L.K., Tang, X.D., Yan, Y.G., Qiao, Q.Q., Zhao, J., and Chen, L.W. 2015. A quasi-linear structure of the southern margin of Eurasia prior to the India-Asia collision: First paleomagnetic constraints from Upper Cretaceous volcanic rocks near the western syntaxis of Tibet, Tectonics, v. 34, no. 7, p. p. 1431-1451. doi:org/10.1002/2014TC003571.

Zhang, L.Y., Ding, L., Pullen, A., Xu, Q., Liu, D.L., Cai, F.L., Yue, Y.H., Lai, Q.Z., Shi, R.D., N. Ducea, M., Kapp, P., and Chapman, A. 2014. Age and geochemistry of western Hoh-Xil-Songpan-Ganzi granitoids, northern Tibet: Implications for the Mesozoic closure of the Paleo-Tethys Ocean, Lithos, no. 190-191, p. p. 328-348. doi:org/10.1016/j.lithos.2013.12.019.

Zhu, D.C., Li, S.M., Cawood, P.A., Wang, Q., Zhao, Z.D., Liu, S.A., and Wang, L.Q. 2016. Assembly of the Lhasa and Qiangtang terranes in central Tibet by divergent double subduction, Lithos, no. 245, p. p. 7-17. doi:org/10.1016/j.lithos.2015.06.023.

Zhu, D.C., Zhao, Z.D., Niu, Y.L., Mo, X.X., Chuang, S.L., Hou, Z.Q., Wang, L.Q., and Wu, F.Y. 2011. The Lhasa Terrane: record of a microcontinent and its histories of drift and growth, Earth and Planetary Science Letters, no. 301, p. p. 241-255. doi:org/10.1016/j.epsl.2010.11.005.

Zhu, D.C., Zhao, Z.D., Pan, G.T., Lee, H.Y., Kang, Z.Q., Liao, Z.T., Wang, L.Q., Li, G.M., Dong, G.C., and Liu, B. 2009a. Early Cretaceous subduction-related adakite-like rocks of the Gangdese belt, southern Tibet: Products of slab melting and subsequent melt-peridotite interaction? Journal of Asian Earth Sciences, v. 34, no. 3, p. p. 298-309. doi:org/10.1016/j.jseaes.2008.05.003.

Zhao, Z., Lu, L., and Wu, Z.H. 2019. Uplifting evolution of the Central Uplift Belt, Qiangtang: constraints from tectono-thermochronology, Earth Sciences Frontiers, v.

26, no. 2, p. p. 249-263. doi:10.13745/j.esf.sf.2018.9.7.

Zhu, D.C., Mo, X.X., Niu, Y.L., Zhao, Z.D., Wang, L.Q., Liu, Y.S., and Wu, F.Y. 2009. Geochemical investigation of Early Cretaceous igneous rocks along an east-west traverse throughout the central Lhasa Terrane, Tibet, Chemical Geology, v. 268, no. 3-4, p. p. 298-312. doi:org/10.1016/j.chemgeo.2009.09.008.

Zhu, D.C., Zhao, Z.D., Niu, Y.L., Dilek, Y., and Mo, X.X. 2011. Lhasa terrane in southern Tibet came from Australia, Geology, 2011, v. 39, no. 8, p. p. 727-730. doi:org/10.1130/G31895.1.

Zhu, D.C., Zhao, Z.D., Niu, Y.L., Dilek, Y., Hou, Z.Q., and Mo, X.X. 2013. The origin and pre-Cenozoic evolution of the Tibetan Plateau, Gondwana Research, v. 23, no. 4, p. p. 1429-1454. doi:org/10.1016/j.gr.2012.02.002.